# The Conformational Flexibility of the Carboxy Terminal Residues 105−114 Is a Key Modulator of the Catalytic Activity and Stability of Macrophage Migration Inhibitory Factor†

Farah El-Turk,‡ Michele Cascella,§ Hajer Ouertatani-Sakouhi,‡ Raghavendran Lakshmi Narayanan,|| Lin Leng,⊥ Richard Bucala,⊥ Markus Zweckstetter,|| Ursula Rothlisberger,§ and Hilal A. Lashuel*,‡

*Laboratory of Molecular Neurobiology and Neuroproteomics, Brain Mind Institute, Ecole Polytechnique Fédérale de Lausanne, CH-1015 Lausanne, Switzerland, Laboratory of Computational Chemistry and Biochemistry, Ecole Polytechnique Fédérale de Lausanne, CH-1015 Lausanne, Switzerland, Department of NMR-Based Structural Biology, Max Planck Institute for Biophysical Chemistry, 37077 Göttingen, Germany, and Yale University School of Medicine, New Haven, Connecticut 06520*

*Received April 5, 2008; Revised Manuscript Received August 5, 2008*

ABSTRACT: Macrophage migration inhibitory factor (MIF) is a multifunctional protein and a major mediator of innate immunity. Although X-ray crystallography revealed that MIF exists as a homotrimer, its oligomerization state *in vivo* and the factors governing its oligomerization and stability remain poorly understood. The C-terminal region of MIF is highly conserved and participates in several intramolecular interactions that suggest a role in modulating the stability and biochemical activity of MIF. To determine the importance of these interactions, point mutations (A48P, L46A), insertions (P107) at the monomer−monomer interfaces, and C-terminal deletion ($\Delta_{110-114}$NSTFA and $\Delta_{105-114}$NVGWNNSTFA) variants were designed and their structural properties, thermodynamic stability, oligomerization state, catalytic activity and receptor binding were characterized using a battery of biophysical methods. The C-terminal deletion mutants ΔC5 huMIF$_{1-109}$ and ΔC10 huMIF$_{1-104}$ were enzymatically inactive and thermodynamically less stable than wild type MIF. Analytical ultracentrifugation studies demonstrate that both C-terminal mutants sediment as trimers and exhibit similar binding to CD74 as the wild type protein. Disrupting the conformation of the C-terminal region 105−114 and increasing its conformational flexibility through the insertion of a proline residue at position 107 was sufficient to reproduce the structural, biochemical and thermodynamic properties of the deletion mutants. P107 MIF forms an enzymatically inactive trimer and exhibits reduced thermodynamic stability relative to the wild type protein. To provide a rationale for the changes induced by these mutations at the molecular level, we also performed molecular dynamics simulations on these mutants in comparison to the wild type MIF. Together, our studies demonstrate that intersubunit interactions involving the C-terminal region 105−114, including a salt-bridge interaction between Arg73 of one monomer and the carboxy terminus of a neighboring monomer, play critical roles in modulating tertiary structure stabilization, enzymatic activity, and thermodynamic stability of MIF, but not its oligomerization state and receptor binding properties. Our results suggest that targeting the C-terminal region could provide new strategies for allosteric modulation of MIF enzymatic activity and the development of novel inhibitors of MIF tautomerase activity.

Macrophage migration inhibitory factor (MIF[1]) is an important proinflammatory and immunoregulatory protein that has been implicated in the pathogenesis of several inflammatory and autoimmune diseases including sepsis (*1, 2*), rheumatoid arthritis (*3, 4*), cancer (*5, 6*), diabetes (*7*), and multiple sclerosis (*8*). MIF also is expressed under physiological conditions in a wide variety of tissues and cell types including neurons (*9, 10*) and is secreted by the anterior pituitary gland as a consequence of the systemic stress response or in response to low concentrations of glucocorticoids (*11, 12*).

Although originally identified as a T cell cytokine that is released after an immune or inflammatory activation and acts to inhibit the random migration of macrophages (*13, 14*), studies over the past two decades have shown that MIF possesses cytokine, enzymatic, hormone, and chaperone-like activities (*15*) and is involved in a wide range of cellular processes, including transcriptional regulation of inflamma-

† Financial support for these studies was provided by the Swiss Federal Institute of Technology Lausanne (H.A.L., F.E.-T., H.O.-S.), a grant from the Swiss National Science Foundation (H.A.L., F.E.-T, 310000-110027), and the National Institutes of Health (L.L., R.B.). NMR work was supported by a DFG Heisenberg grant (ZW 71/2-1 and 71/3-1) to M.Z.

* To whom correspondence should be addressed. E-mail: hilal.lashuel@epfl.ch. Phone: (41) 21 69 39 691. Fax: (41) 21 31 780.

‡ Laboratory of Molecular Neurobiology and Neuroproteomics, Brain Mind Institute, EPFL.

§ Laboratory of Computational Chemistry and Biochemistry, EPFL.

|| Max Planck Institute for Biophysical Chemistry.

⊥ Yale University School of Medicine.

[1] Abbreviations: MIF, macrophage migration inhibitory factor; CD, circular dichroism; SEC, size-exclusion chromatography; AUC, analytical ultracentrifugation; MALDI, matrix-assisted laser desorption ionization; HSQC, heteronuclear single quantum coherence; GdnHCl, guanidine hydrochloride; MD, molecular dynamics; wt, wild-type.

10.1021/bi800603x CCC: $40.75 
Published on Web 09/17/2008

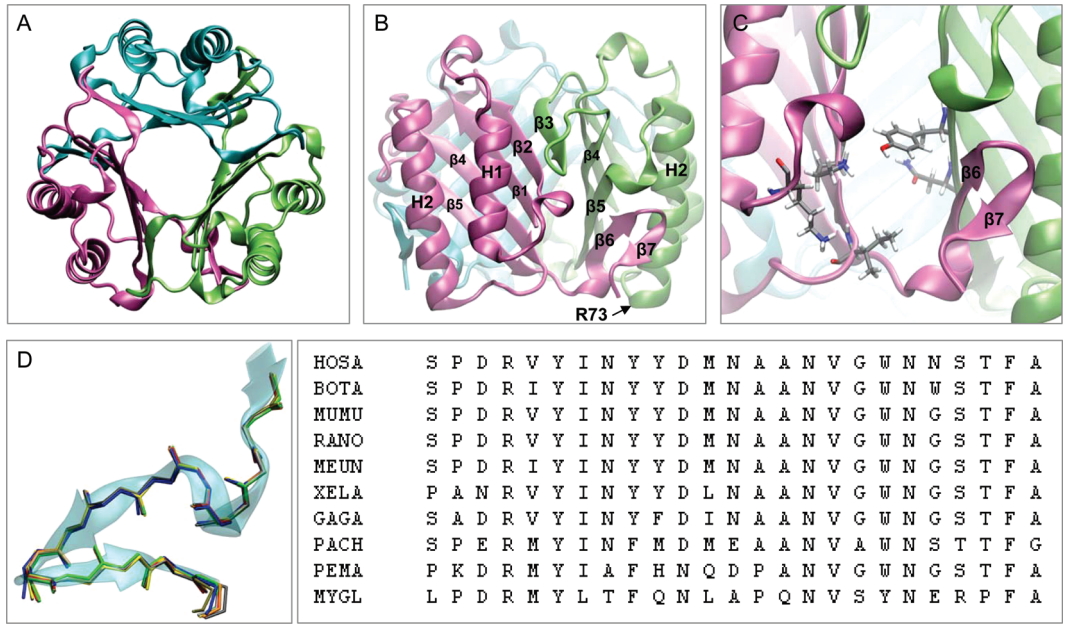


FIGURE 1: Structure of wt huMIF trimer: (A) top view; (B) side view. The three monomers are represented as cartoons and are colored in cyan, magenta and lime. (C) Side view of the trimer illustrating the relative positions of the catalytic site and the C-terminal strands $\beta$6 and $\beta$7. Structural data according to ref *24*; pdb code 1GD0. (D) Primary structure homology of different MIF species; structural data according to the pdb codes 1CA7 and 1GD0 (human MIF); 1MFF (mouse MIF); 1P1G (variant of human MIF); 2GDG (variant of mouse MIF); 1UIZ (MIF from *Xenopus laevis*); and 2OS5 (MIF from *Ancylostoma ceylanicum*). Figures were generated with VMD (Visualization Molecular Dynamics) software (*53*).

tory gene products (*16*), cell cycle control (*17, 18*), modulation of cell proliferation and differentiation (*19*), regulating glucocorticoïd activity (*20*), inactivation of p53 tumor suppressor factor (*21*) and signal transduction. However, the molecular mechanisms and structural basis underlying each of these functions remain poorly understood. Therefore, better understanding of the structural activity relationship of MIF is critical for elucidating the molecular basis underlying many of its biochemical and biological activities as well as its role in disease.

MIF is known to possess two enzymatic activities: it can act both as a keto−enol tautomerase and a thiol-protein oxidoreductase. As a tautomerase, MIF catalyzes the keto−enol tautomerization of D-dopachrome (*22*) and phenylpyruvate (or hydroxyphenylpyruvate) (*23, 24*). As a thiol-protein oxidoreductase, MIF catalyzes the reduction of insulin and 2-hydroxyethyldisulfide (HED) by glutathione (GSH) and dihydrolipoamide (DHL) (*25, 26*). However, the physiological relevance of the catalytic activities of MIF and their role in regulating its various biological functions remain controversial. Furthermore, the natural substrates of MIF are yet to be identified.

X-ray crystallographic and NMR studies demonstrate that MIF exists predominantly as a homotrimer with dimensions of approximately 35 × 50 × 50 Å (*27, 28*). Each monomer consists of 114 amino acid residues (MW ∼ 12.3 kDa) and exists as an $\alpha/\beta$ structure composed of two antiparallel α-helices packed against a four-stranded $\beta$-sheet (Figure S1; see Supporting Information). The subunits interact via intersubunit $\beta$-sheet contacts to form a symmetrical $\beta$-barrel trimer with a solvent exposed central channel. The C-terminal region of MIF comprising residues 105−114 is involved in several intersubunit interactions and has been proposed to be critical for trimer formation and stability (*29*−*31*). X-ray crystallographic studies of MIF bound to its unnatural substrates revealed that the tautomerase active site is formed at the monomer−monomer interfaces and involves amino acid residues from both neighboring subunits, whereas the oxidoreductase activity is modulated by CALC motif (Cys57-Ala-Leu-Cys60) within the $\beta$-strand $\beta$4 (Figure 1B) of each monomer (*24, 25, 32*).

Despite the extensive knowledge about the structure of the MIF trimer, very little is known about the molecular and structural determinants that govern the oligomerization of MIF and the role of quaternary structure in modulating its functions in health and disease. Previous structure activity studies focused mainly on using site-directed mutagenesis to elucidate the role of the N and carboxy terminal residues in modulating the enzymatic activity and immunologic functions of MIF. Two prior studies suggested that deletion of the last 5−10 C-terminal residues does not affect the overall structural stability of MIF, but reduces its enzymatic and macrophage activating properties (*31*). However, the molecular and structural basis underlying the biochemical and functional consequences of these mutations and their effect on the oligomerization state of MIF remains unknown.

Motivated by our interest in elucidating the role of quaternary structure in modulating the activity of MIF in health and disease, we sought to understand the relative importance/contribution of intersubunit interactions involving the C-terminus and elucidate the relationship between the conformational flexibility of this region and the catalytic activity and trimer stability of MIF. Deletion and point mutation variants were generated to determine the consequences of attenuating these intersubunit interactions on the secondary structure, tertiary structure, oligomerization state, enzymatic activity, thermodynamic stability and receptor binding properties of MIF *in vitro*. Our findings provide new insight into the role of the carboxy terminal residues 105−114 in modulating the structural flexibility of MIF and

suggest novel strategies for selective targeting of MIF biochemical and immunologic functions based on modulating its conformational and/or oligomerization states.

## MATERIALS AND METHODS

*Materials.* Polymerase chain reaction (PCR) and other molecular biology reagents were purchased from Stratagene unless stated otherwise. DNA mini and maxi prep reagents were purchased from Qiagen and oligonucleotide primers from Microsynth. *Escherichia coli* BL21 (DE3) cells, rabbit monoclonal anti-huMIF and goat antirabbit ALEXA Fluor 680 were purchased from Invitrogen. Miscellaneous chemicals were from Sigma-Aldrich Chemicals and were of the highest grade commercially available. Isopropyl 1-thio-$\beta$-D-galactopyranoside (IPTG) was purchased from Applichem. $^{15}$N-Ammonium chloride and $^{13}$C-glucose were purchased from CIL (Cambridge Isotope Laboratories, Switzerland).

*Site-Directed Mutagenesis of C-Terminal Truncated huMIF.* Wt huMIF was amplified from Jurkat H33HJ-JA1 T cell DNA and cloned into the pET11b expression vector as described previously (*33*). C-Terminal truncated huMIF, $\Delta$C5 huMIF$_{1-109}$ and $\Delta$C10 huMIF$_{1-104}$, A48P huMIF and P107 huMIF mutants were engineered by site directed mutagenesis using mutagenesis kit from Stratagene. C-Terminal truncations were designed to have either the last five amino acids (NSTFA) or the last ten amino acids (NVGWNNSTFA) deleted. All mutants of huMIF were cloned from huMIF-pETllb by DNA amplification. Polymerase chain reactions (PCR) were performed in a Px2 Thermal Cycler (Catalys AG, a Promega Company). Initial denaturation was for 30 s at 95 °C followed by $x$ cycles of 30 s at 95 °C, 1 min at 55 °C, and (1 min/Kb of plasmid length) at 68 °C using 2.5 units of Pfu Turbo DNA polymerase (Stratagene) ($x = 18$ for C-truncated mutants and $x = 16$ for A48P and P107 mutants). Primers designed were 5′ GTG GGC TGG AAC TAA GAG CCG CAG G 3′ (sense), 5′ C CTG CGG CTC TTA GTT CCA GCC CAC 3′ (antisense) for C5 huMIF$_{1-109}$; 5′ CGA CAT GAA CGC GGC CTA AGA GCC GCA GG 3′ (sense) and 5′ CC TGC GGC TCT TAG GCC GCG TTC ATG TCG 3′ (antisense) for $\Delta$C10 huMIF$_{1-104}$; and 5′ CGG ACC AGC TCA TGC CGT TCG GCG GCT CC 3′ (sense) and 5′ GG AGC CGC CGA ACG GCA TGA GCT GGT CCG 3′ (antisense) for A48P huMIF; and 5′ GCG GCC AAT GTG CCG GGC TGG AAC 3′ (sense) and 5′ GTT GTT CCA GCC CGG CAC ATT GGC 3′ (antisense) for P107 huMIF. Mutants DNA sequences were confirmed by sequencing at Microsynth by using T7 primer (http://www.microsynth.ch/).

*Expression and Purification of Wt and Mutant huMIF.* HuMIF-containing pETllb plasmid DNA was used to transform the *E. coli* BL21 (DE3). One liter of culture was grown at 37 °C until the optical density at 600 nm reached 0.6−0.65 and induced with isopropyl 1-thio-$\beta$-D-galactopyranoside (IPTG) to a final concentration of 1 mM. After 4 h at 37 °C, bacteria were harvested and the cell pellets were frozen at −20 °C until use. For protein purification, the bacterial pellets (~4.7 g for 1 L of culture) were thawed and resuspended in 24 mL of lysis buffer (Tris 50 mM, KCl 50 mM, MgAc 5 mM, sodium azide 0.1%, pH 8.5) and lyzed by sonication (Sonics Vibra Cell) for 20 min, then harvested by centrifugation for 25 min at 10 000 rpm (4 °C). Supernatant containing huMIF was recovered and sterile-filtered through a 22 $\mu$m membrane filter. All proteins were purified using a two step purification strategy using anion exchange and size exclusion chromatography that have been optimized to yield highly pure proteins (>95%). The supernatant was loaded onto a Mono Q anion exchange column (HiPrep 16/10 Q FF) and eluted using a linear NaCl gradient (0.15−1.00 M NaCl) in 25 mM Tris buffer (pH 7.6) using a fast protein liquid chromatography system (FPLC, AKTA Explorer1 Amersham Pharmacia Biotech). Wt and mutants huMIF elute with the flow through fractions. MIF-containing fractions were pooled, concentrated and injected onto a Superdex 75 16/60 size exclusion chromatography column equilibrated with Tris-buffered saline (25 mM Tris, 150 mM NaCl, pH 7.6). HuMIF containing fractions were pooled and concentrated to the desired concentrations and kept at 4 °C until use. All experiments with the C-terminal truncated mutants were performed after filtering through 0.22 $\mu$m filters and within two weeks from purification.

For preparation of uniformly [$^{15}$N]-labeled and $^{13}$C/$^{15}$N-double-labeled huMIF, samples were prepared by growing the bacteria on M9 minimal containing $^{15}$N-ammonium chloride (1 g/L) as the only nitrogen source, or $^{15}$N-ammonium chloride and $^{13}$C-glucose in case of double labeled samples, supplemented with minerals and cofactors (*34*).

*SDS−PAGE Analysis.* SDS−PAGE was performed under reducing conditions. Protein samples were mixed with one volume of the SDS sample buffer. 15 % gels (54 cm$^2$) were employed, and a voltage of 180 V was applied. The gels were stained with coomassie blue and/or silver staining (SilverXpress Silver Staining Protocols, Invitrogen), according to the manufacturer protocol.

*Native PAGE.* Native PAGE analysis was performed with the Phast system on polyacrylamide mini gels type PhastGel High density (ref. 17-0679-01, GE Healthcare) using native buffer strips (Pharmacia Biotech). The Phast gel was prerun at 250 V and 15 °C for 10 V h. Samples (1 $\mu$L) were loaded at 250 V for 1 V h and electrophoresis was carried out at 400 V, 15 °C for 1600 V h. The gel was then stained with silver staining.

*MIF Keto−Enol Tautomerase Activity.* The keto−enol tautomerase activity of MIF was determined by measuring the rate of formation of enol form of D-dopachrome methyl ester and phenylpyruvate as model catalytic substrates of MIF. MIF tautomerase activity using the D-dopachrome substrate was performed as described previously (*22*). D-Dopachrome methyl ester was freshly prepared by reaction of periodate ($NaIO_4$) (8 mM) on L-3,4-dihydroxyphenylalanine methyl ester (4 mM) for 5 min at room temperature and then placed directly on ice before use. MIF activity was then determined at room temperature by adding different concentrations of D-dopachrome methyl ester to a cuvette containing 50 mM potassium phosphate buffer, pH 6.0, and 0.5 mM EDTA. After 30 s approximately, 25 nM MIF was added to the cuvette and resulted in a decrease in absorbance at 475 nm that was followed for 1 min using a spectrophotometer (CARY 100 Bio UV−visible spectrophotometer). Data presented are the average of at least 3 measurements.

MIF tautomerase activity using the phenylpyruvate substrate was performed as described previously (*35*). The enolase reaction of phenylpyruvate was assessed at room

temperature by monitoring the increase in absorbance at 300 nm using the same spectrophotometer as before. The reaction mixture contained in reaction buffer (200 mM sodium phosphate, pH 6.2) 0.9 M boric acid and different concentrations of the substrate (ketone form of phenylpyruvate) prepared freshly in reaction buffer. 25 nM huMIF was added, and the reaction was followed for 10 min. Initial rate of catalytic activity was calculated within the first 30 s of the reaction. Data presented are the average of at least 3 measurements.

*Probing the Conformational and Thermodynamic Stability of MIF by Circular Dichroism and Fluorescence Spectroscopy.* The far-UV (195−250 nm) CD spectra of wt and mutant huMIF in PBS 1X (137 mM NaCl, 10 mM phosphate, 2.7 mM KCl, pH 7.4) were recorded at RT using a 0.1 cm quartz cell and Jasco J-815 CD spectrometer equipped with a thermostatted cell holder. Data were acquired at a step size of 0.2 nm, an averaging time of 0.5 s, a bandwidth of 0.5 nm, and an average of three scans recorded to generate the data reported in units of ellipticity. Thermal denaturation (TD) studies were performed by recording the mean molar ellipticity at 218 nm for each protein (14 $\mu$M) in PBS 1X as a function of the temperature (20−95 °C). The spectra represent the average of at least 3 scans. Data were collected using a temperature slope of 2 °C/min with data pitch of 0.2 °C and a bandwidth of 1 nm. Unfolding curves are expressed as the percentage of unfolded protein relative to native protein (i.e., the change in ellipticity at 218 nm) over the increase in temperature. Guanidine hydrochloride (GdnHCl) induced denaturation studies were performed by recording the mean molar ellipticity per residue as a function of wavelength (195−240 nm) and GdnHCl concentration. The spectra represent the average of at least 3 scans performed on the protein sample (14 $\mu$M) in PBS 1X buffer at RT. Scans were collected at 0.2 nm intervals with a bandwidth of 1 nm and a time constant of 0.5 s. Unfolding curves are expressed as the percentage of unfolded protein relative to native protein (i.e., the change in ellipticity at 218 nm) over GdnHCl concentration. All far-UV CD data were smoothed using a Steinman function (Kaleidagraph software), which reduced the noise without perturbing the appearance of the data.

Guanidine hydrochloride induced denaturation studies were also performed by monitoring changes in the fluorescence emission maximum of wt and C-truncated mutants as a function of GdnHCl concentration. The spectra represent the average of at least 3 scans performed on the protein sample (3 $\mu$M wt huMIF and $\Delta$C5 huMIF$_{1-109}$; 5 $\mu$M $\Delta$C10 huMIF$_{1-104}$) in PBS 1X incubated overnight at RT with different concentrations of GdnHCl. The wt huMIF and $\Delta$C5 huMIF$_{1-109}$ mutant were excited at 295 and 280 nm, whereas an excitation wavelength of 280 nm only was used for the $\Delta$C10 huMIF$_{1-104}$ mutant, which lacks the only tryptophan residue in wt huMIF (Trp108). Fluorescence emission was acquired over a wavelength range of 290−450 nm using a LS 55 Perkin-Elmer fluorescence spectrometer. Unfolding curves are expressed as the percentage of unfolded protein relative to native protein (i.e., the change in fluorescence emission intensity at 342 nm for wt huMIF, 350 nm for $\Delta$C5 huMIF$_{1-109}$ and 312 nm for $\Delta$C10 huMIF$_{1-104}$) as a function of GdnHCl concentration.

*1-Azido-5-naphthalene Sulfonyl (ANS) Binding Studies.* To evaluate the relative exposure of hydrophobic residues within wt and C-truncated mutants, 7 $\mu$M of purified and dialyzed proteins (in PBS 1X) were incubated for 15 min in the presence of 50 $\mu$M of ANS at RT. A stock ANS solution of 10.54 mM in PBS 1X was freshly prepared, and its concentration was determined by UV using the extension coefficient of ANS at 351 nm ($\varepsilon_{351\ nm} = 6240\ M^{-1}\ cm^{-1}$). Fluorescence intensities were measured by excitation at 410 nm and emission was acquired over a wavelength range of 420−600 nm using a LS 55 Perkin-Elmer fluorescence spectrometer.

*Quaternary Structure Determination by Size Exclusion Chromatography (SEC) and Analytical Ultracentrifugation (AUC).* Size exclusion chromatography experiments were performed on purified samples using an analytical Superdex 75 10/30 column which has an optimal separation range of peptides and proteins with molecular weight ranging from 3 to 70 kDa. The column was equilibrated with 10 mM Tris buffer (pH 7.6), and MIF samples (12 $\mu$M in PBS 1X) in volumes of 0.5 mL were injected onto the column and eluted at a flow rate of 0.4 mL/min in a Waters 2795 analytical HPLC system equipped with a photodiode array detector. Analytical ultracentrifugation experiments were performed on purified and dialyzed MIF samples (12 $\mu$M in PBS 1X) on a Beckman Optima XL-A analytical ultracentrifuge. Sedimentation velocity experiments were carried out at 20 °C using 380−400 $\mu$L of protein solution. Data were recorded at rotor speeds of 50 000 rpm in continuous mode at 21 °C with a step size of 0.003 cm. The experimentally determined partial specific volume of 0.765 mg/mL was used for calculating the molecular weights of wt and mutants huMIF (*36*). Given that this value was determined only for wt huMIF and for comparison purposes, the molecular weights of the mutants were also determined using the calculated (using the program SEDNTERP (*36*)) partial specific volumes of 0.7347 mL/g, 0.7364 mL/g, and 0.7332 mL/g for $\Delta$C5 huMIF$_{1-1.09,}$ $\Delta$C10 huMIF$_{1-104}$ and P107 huMIF. The sedimentation velocity absorbance profiles were analyzed as a $c(s)$ distribution of the Lamm equation using SEDFIT (*37*). To obtain the molecular weights, the molar mass distributions $c(M)$ were obtained by transforming the corresponding $c(s)$ using SEDFIT.

*Light Scattering.* Static light scattering was used to probe the oligomerization state of wt and C-terminal deletion mutants of MIF. All measurements were performed at room temperature on a DAWN HELLIOS multiangle light scattering detector (Wyatt Technology Corp, Santa Barbara CA) online with a size exclusion chromatography column. The system is also equipped with UV and refractive index detectors. 50−100 $\mu$L of sample in SEC buffer was injected onto Superdex 75 10/30 column and eluted at a flow rate of 0.5 mL/min. Absolute MWs were determined using ASTRA version 5.3 from Wyatt Technologies.

*NMR Spectroscopy.* NMR spectra were acquired at 27 °C on Bruker Avance 600 and 800 MHz NMR spectrometers using a triple-resonance cryoprobe equipped with $z$-axis self-shielded gradient coils. Wt human MIF measurements were done on a 100 $\mu$M samples. For triple-resonance experiments, $\Delta$C5 huMIF$_{1-109}$ and $\Delta$C10 huMIF$_{1-104}$ were concentrated to 200 $\mu$M, whereas HSQCs of the mutants were recorded at 60 $\mu$M protein concentration. To probe for aggregation,

additional NMR spectra were recorded for ΔC10 huMIF$_{1-104}$ at a concentration of 10 $\mu$M. All samples were in 20 mM $Na_2HP0_4$, 0.5 mM EDTA, 0.02% $NaN_3$ (pH 7.0) and 10% $D_2O$. Two-dimensional $^1H-^{15}N$ heteronuclear single quantum coherence (HSQC) spectra were recorded using 256 × 1024 complex data points in F1 and F2 dimensions with a relaxation delay of 1.0 s. 48 scans per increment were recorded for the wt protein whereas 64 scans were recorded for the truncation mutants. Spectral widths were 2200 and 8950 Hz in $^{15}N$ and $^1H$ dimensions, respectively. For backbone assignment of ΔC5 and ΔC10 truncated huMIF, 3D HNCA experiments were recorded on a 800 MHz spectrometer using a cryoprobe. Spectra were processed with XWIN-NMR and NMRPipe. Visualization and manipulation were performed using the public domain graphics program Sparky 3.

*MIF Receptor Binding Assay.* Recombinant, soluble huMIF receptor ectodomain (sCD74$^{73-232}$) was cloned and purified as described in ref *38* and used to coat 96 well plates by incubation at 4 °C overnight. Plates were washed 4 times with TTBS (pH 7.4) and blocked with superblock buffer (PIERCE) for 1 h at room temperature. Biotinylated huMIF (Roche Molecular Biochemical) was prepared and added together in triplicate wells with increasing concentrations of purified native huMIF (*33*), heat-denatured huMIF, or test MIF proteins. Incubation was at room temperature for 2 h. After washing wells 4 times with TTBS (pH 7.4), streptavidin-conjugated alkaline phosphatase (R&D) was added, incubation continued for an additional hour, and the wells washed and bound complexes detected by adding *p*-nitrophenyl phosphate (Sigma). Absorbance was read at 405 nm using a DYNATECH, MR5000 plate reader, and values plotted as percent $OD_{405}$ relative to wells containing biotinylated-MIF alone. The plots shown are representative of at least three assays, and each plotted point depicts a SEM < 10%.

*Mass Spectrometry.* Mass spectrometric analysis of huMIF was performed by matrix-assisted laser desorption ionization MALDI MS using a linear positive ion mode on ABI 4700 (PAF Lausanne). Linear mode calibration was applied with single point on α-synuclein wild type ($MH^+$: 14461.19). Sample preparation: After desalting huMIF sample on a StageTip C18 (Proxeon), one volume of sample was mixed with one volume of matrix. Matrix solution consists of 20 mg/mL of dihydroxybenzoic acid in 1% phosphoric acid/acetonitrile 1/1. A two-layer sample preparation has been selected for the MW analysis.

*Computational Studies.* Classical molecular dynamics (MD) simulations were based on the X-ray structure of huMIF (pdb code 1GD0) determined at 1.5 Å resolution (*27*); residues corresponding to the His-tag sequence were removed from the pdb file. Three model systems of the trimeric structure of MIF were considered: wt huMIF, ΔC5 huMIF$_{1-109}$, and ΔC10 huMIF$_{1-104}$. Protonation states of titratable groups were assigned according to empirical p$K_a$ prediction (*39*) and Poisson−Boltzmann calculations (*54*). Chlorine anions were added to neutralize the charge of the models. Wt huMIF, ΔC5 huMIF$_{1-109}$, and ΔC10 huMIF$_{1-104}$ models were solvated by 3 chlorine anions and 13654, 13483 and 13745 water molecules, respectively. MD calculations were carried out with the SANDER module of the AMBER8 suite of programs (*40*). The AMBER (parm98) (*41*) and TIP3P (*42*) force fields were used for the protein atoms and for water, respectively. Periodic boundary conditions were applied. Electrostatic interactions were calculated with the Ewald particle mesh method (*43*). A 12 Å cutoff for van der Waals interactions was used. Bonds involving hydrogen atoms were constrained using the SHAKE algorithm (*44*). A time step of 1.5 fs was used during the dynamics. Constant temperature and pressure conditions were achieved by coupling the systems with a Berendesen thermostat and barostat. Our computational protocol for the three models was the following: (i) equilibration of the solvent by 200 ps of MD at ambient conditions (310 K temperature and 1 atm pressure), while keeping the protein fixed; (ii) energy minimization of the entire system through 25 steepest descent steps and 30000 conjugate gradient steps, progressively allowing hydrogen atoms, side chain atoms and backbone atoms to move; (iii) thermalization of the whole systems by MD calculations: 30 ps from 0 to 50 K, 45 ps from 50 to 150 K, 70 ps from 150 to 310 K; (iv) 10 ns of MD simulations at 310 K and 1 atm.

## RESULTS

*Mapping of Intersubunit Interactions Involved in Trimer Formation and Stability.* To identify key intersubunit contacts that are important in modulating trimer formation and stability, we examined high-resolution X-ray structures of MIF and analyzed hydrogen-bonding, hydrophobic and salt-bridge interactions that define the monomer−monomer interfaces. The crystal structures reveal several intersubunit interactions that are likely to contribute to trimer formation and stability (Figures 1B and S1; see Supporting Information): (1) Formation of intermolecular antiparallel β-sheet between β-strand β3 of one monomer and the edge β-strand β2 of the neighboring monomer (Figures 1B and S1; see Supporting Information). This β-sheet is stabilized mainly by hydrogen bond interactions between residues Val39 (in β2, monomer 1) and Ala48 (in β3, monomer 2). (2) The C-terminal β-hairpin comprising residues 105−114 is involved in several intersubunit interactions and could contribute to trimer stabilization through two types of contacts: (i) intersubunit β-sheet formation mediated by hydrogen bonding between Asp105 and Gly107 in the C-terminal β-strand β6 and Ile96 and Tyr98 within the inner β-strand β5 of the neighboring subunit, (Figures 1B and S1; see Supporting Information); (ii) by a salt-bridge interactions between the carboxylate group of the C-terminal residue Ala114 and the side-chain of Arg73, located on the α-helix H2 of the neighboring subunit (Figures 1B and S1; see Supporting Information).

Comparison of the crystal structures of human and rat MIF reveals that the rat MIF trimer is virtually identical to that of huMIF despite the fact that its entire C-terminal region (corresponding to residues 105−114 in human MIF) appears to be unstructured (*45*). These findings suggest that the C-terminal region may not be required for trimer formation and stability. However, the location of the active site at the monomer−monomer interface and the interactions between the C-terminal strand β6 and β5, which contains several residues that participate in substrate recognition and catalysis (Figure 1C), suggest that the C-terminal region may significantly influence the structural and dynamic properties as well as biochemical and biological activities of MIF.

In order to understand the relative importance of the various interactions involving the C-terminal region in the oligomerization, thermodynamic stability, and function of huMIF, we used site-directed mutagenesis to generate single site and C-termini-truncated mutants of huMIF and characterized these mutants using an array of biochemical and biophysical methods. To probe the importance of the salt-bridge interaction between Ala114 and Arg73, we generated a mutant where the last five amino acids (ΔNSTFA), corresponding to the $\beta$-strand $\beta$7, were removed (Figure 1B). We hypothesized that this would significantly increase the distance between the two interacting groups and disrupt the formation of the salt bridge. To determine the effect of disrupting all stabilizing interactions involving the C-terminal $\beta$-strands (salt-bridge interaction between Ala114 and Arg73 as well as the intersubunit hydrogen bonds between $\beta$-strands $\beta$6 and $\beta$5), we generated a mutant where the entire $\beta$-hairpin comprising the $\beta$-strands $\beta$6 and $\beta$7 (ΔNVGWNNSTFA) was removed (Figure 1B). To determine the contribution of the hydrogen bonding interactions between Ala48 ($\beta$3) and Val39 ($\beta$2), we generated a mutant in which Ala48 was replaced by the secondary structure breaker proline residue (A48P).

*Protein Expression and Purification.* Wt and mutant huMIF were expressed in *E. coli* BL21 (DE3) cells and purified to purity using the protocol described in Materials and Methods. The wt and C-terminal deletion mutants expressed as soluble proteins and migrated as a single band on reducing SDS−PAGE. The identity and purity of expressed proteins were verified by SDS−PAGE/silver staining and Western blot and mass spectrometry (data not shown). MALDI-TOF analyses revealed single peaks corresponding to the predicted molecular weight of wt huMIF (12.345 kDa), ΔC5 huMIF$_{1-109}$ (11.825 kDa), and ΔC10 huMIF$_{1-104}$ (11.254 kDa). The A48P huMIF mutant expressed in *E. coli* as inclusion bodies, supporting the conclusion that it failed to fold properly. It is also possible that A48P aggregation is mediated by misfolding of the trimer, although attempts to reconstitute the native trimer from purified and lyophilized protein were not successful. This observation suggests that the intersubunit $\beta$-sheet involving the $\beta$-strands $\beta$3 from one monomer and $\beta$2 from the adjacent monomer contribute significantly to trimer formation and stability.

*Probing the Effect of Carboxy-Terminal Truncation on the Functional Properties of huMIF.* To determine the effect of the carboxy-terminal deletions on the functional properties of huMIF, we compared the enzymatic activity and receptor (CD74) binding properties of wt and mutants huMIF.

*Catalytic Activity.* The catalytic activity of wt and mutant huMIF were studied using D-dopachrome and phenylpyruvate as substrates. Both ΔC5 huMIF$_{1-109}$ and ΔC10 huMIF$_{1-104}$ did not show any detectable tautomerase activity with D-dopachrome (Figure 2A) and phenylpyruvate (Figure 2B) as substrates. Even at higher protein concentrations (up to 10 $\mu$M) both mutants exhibited very minimal, if any, catalytic activity.

*Receptor (CD74) Binding.* Although the molecular mechanisms underlying the biological functions of MIF remain poorly understood, MIF's binding to CD74, a type II transmembrane protein, was demonstrated to be essential for several of MIF's cellular functions such as activation of ERK 1/2 MAPK cascade (*38*) and cell proliferation (*46*). Moreover, recent studies by Meyer-Siegler et al. showed that MIF−CD74 interaction mediates bladder inflammation and inhibition of MIF or CD74 attenuates growth and invasion of prostate cancer cells (*47, 48*). Interestingly, all three proteins wt huMIF, ΔC5 huMIF$_{1-109}$, and ΔC10 huMIF$_{1-104}$ displayed virtually identical binding to CD74 (Figure 2C−E), indicating that the C-terminal residues 105−114 may not be directly involved in the binding to CD74.

*Biophysical Characterization of Wt and C-Terminal Truncated huMIF Mutants.* In order to understand the molecular basis underlying the loss of enzymatic activity upon deletion of the C-terminal residues 110−114 ($\beta$6) and 105−114 ($\beta$6 and $\beta$7), we probed the effect of C-terminal truncation on the conformational properties and thermodynamic stability of huMIF by far-UV circular dichroism. The CD spectra of the wt and C-terminal deletion mutants showed a broad negative ellipticity between 225 and 208 nm, consistent with the presence of a mixture of α-helix and $\beta$-sheet structures (Figure 3A). The spectra of both ΔC5 huMIF$_{1-109}$ and ΔC10 huMIF$_{1-104}$ were shifted toward lower wavelengths and exhibited a slight decrease in ellipticity at 218−220 nm, consistent with the expected disruption of the C-terminal $\beta$-hairpin upon deletion of the C-terminal $\beta$-strands.

*The C-Terminal Deletion Mutants Are Thermodynamically Less Stable than Wt huMIF.* To understand the role of the C-terminal region in modulating the stability of MIF, we compared the stability of wt and C-terminal deletion mutants to thermal and GdnHCl induced denaturation. Thermal denaturation of wt and C-terminal deletion mutants monitored by far-UV CD (at 218 nm) showed a cooperative unfolding with increasing temperature. As shown in Figure 3B, ΔC5 huMIF$_{1-109}$, and ΔC10 huMIF$_{1-104}$ began to undergo conformational changes at lower temperatures than wt huMIF ($T_m$ = 79 °C) and displayed $T_m$ values of 69.5 and 71.5 °C respectively. Over the concentration range of 2.5−50 $\mu$M, we did not observe any change in the $T_m$ values for all three proteins (Figure S3, see Supporting Information). The thermal denaturation of all three proteins was irreversible due to protein aggregation which occurs upon unfolding of MIF.

To further investigate the effect of the carboxy terminus on trimer stabilization and conformational stability of huMIF, GdnHCl-induced unfolding studies were performed on wt and C-terminal truncated huMIF mutants. GdnHCl-induced unfolding of MIF was monitored by far-UV CD and fluorescence spectroscopy. Wt and mutants huMIF exhibited a cooperative unfolding curves with midpoints of unfolding ($C_m$) of 2.14 M, 1.82 and 2.06 M GdnHC1 for wt huMIF, ΔC5 huMIF$_{1-109}$, and ΔC10 huMIF$_{1-104}$, respectively (Figure 3C), in agreement with the order of stability determined by thermal denaturation. GdnHCl-induced denaturation was also studied by fluorescence spectroscopy. MIF has only one tryptophan (W108) residue that is located within the C-terminal region under investigation; only ΔC10 huMIF$_{1-104}$ lacks W108. Therefore, we also monitored the unfolding of all proteins using excitation wavelengths of 280 nm. Using an excitation wavelength of 280 nm, we obtained midpoints of denaturation of 1.80, 1.20 and 2.00 M GdnHCl for wt huMIF, ΔC5 huMIF$_{1-109}$, and ΔC10 huMIF$_{1-104}$, respectively (Figure 3D). Using an excitation wavelength of 295 nm, we obtained similar midpoints of denaturation for wt huMIF

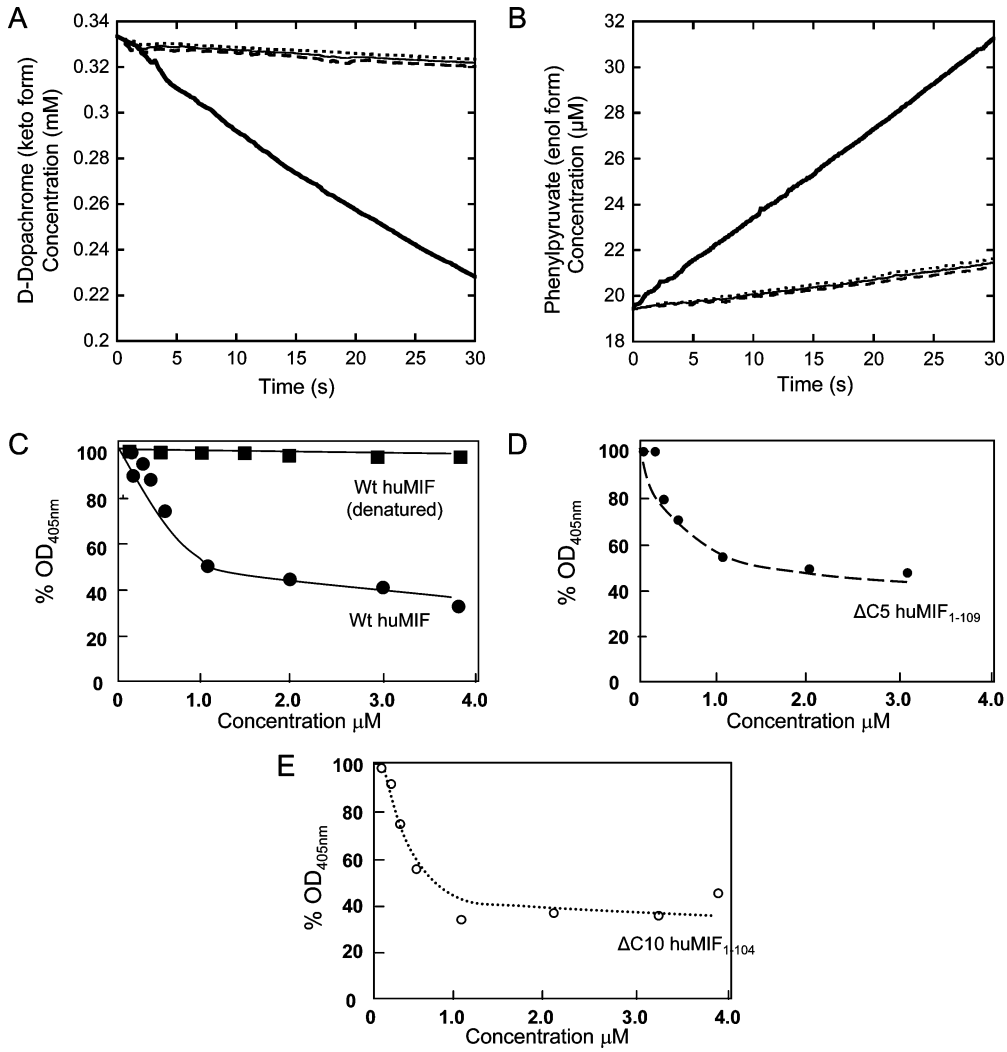


FIGURE 2: Removal of the C-terminal amino acids corresponding to $\beta$6 and/or $\beta$7 strand(s) abolishes the enzymatic activity of MIF (A, B), but has no effect on receptor binding (C−E). D-Dopachrome (A) and phenylpyruvate (B) tautomerization in the presence of wt huMIF (solid line), ΔC5 huMIF$_{1-109}$ (dashed line) and ΔC10 huMIF$_{1-104}$ (dotted line). Thin solid lines correspond to the substrate in the absence of MIF. Wt huMIF and C-truncated mutants exhibit similar binding to CD74 receptor. All three proteins (wt huMIF (C), ΔC5 huMIF$_{1-109}$ (D) and ΔC10 huMIF$_{1-104}$ (E)) bind equally to CD74. Under denaturing conditions, MIF does not bind to CD74. CD74 binding to MIF was measured as a percentage of $OD_{405}$ relative to biotinylated-MIF alone (see Materials and Methods).

(1.80 M) and ΔC5 huMIF$_{1-109}$ (1.2 M). Interestingly, the $C_m$ values obtained by fluorescence spectroscopy are slightly lower than those obtained by far-UV CD, possibly due to the fact that the residues being monitored (Tyr and Trp) are located in regions that are more accessible and conformationally less stable.

*ANS Binding.* To further probe tertiary structure changes induced by deletion of the C-terminal residues, we performed ANS binding studies on the wt and C-terminal huMIF mutants. ANS binds to accessible hydrophobic surfaces of proteins and thus provides a measure of the relative exposure of hydrophobic residues. ANS binding is reported by an increase in ANS fluorescence emission when excited at 410 nm as well as by a blue shift in the fluorescence emission maximum. ANS binding was determined under the same experimental conditions (i.e., protein concentrations, pH, buffer conditions, and temperature). Figure 3E demonstrates that both mutants exhibit higher fluorescence intensity than the wt protein with ΔC5 huMIF$_{1-109}$ exhibiting the highest ANS fluorescence (ΔC5 huMIF$_{1-109}$ > ΔC10 huMIF$_{1-104}$ > wt huMIF), suggesting an increased exposure of the hydrophobic surfaces of ΔC5 huMIF$_{1-109}$ compared to ΔC10 huMIF$_{1-104}$ and wt huMIF, consistent with simulations, where the ΔC5 huMIF$_{1-109}$ mutant is less packed than both the wt and ΔC10 huMIF$_{1-104}$ isoforms (see below).

*Probing the Effect of the C-Terminal Deletions on the Oligomerization State of MIF.* The loss of catalytic activity and decreased stability of the C-terminal deletion mutants combined with the fact that the tautomerase active site is formed at the monomer−monomer interfaces of the trimer (*24*) led us to hypothesize that the loss of intersubunit stabilizing interactions involving the C-terminal residues 105−114 may result in disruption of the native quaternary structure of MIF. To test this hypothesis we compared the quaternary structure distribution of wt huMIF, ΔC5 huMIF$_{1-109}$, and ΔC10 huMIF$_{1-104}$ at 12 $\mu$M by sedimentation velocity analytical ultracentrifugation. Figure 4B shows that wt and C-terminal deletion mutants huMIF sediment predominantly (>95%) as a single species with experimental sedimentation coefficients of 3.15 S (±0.1 S) for wt huMIF, 3.06 S (±0.1 S) for ΔC5 huMIF$_{1-109}$ and 2.97 S (±0.1 S) for ΔC10 huMIF$_{1-104}$. Using the partial specific volume measured by Philo et al. (0.765 mL/g (*36*)) we obtained molecular weights of 37.4 kDa, 39.1 kDa and 38.2 kDa, for

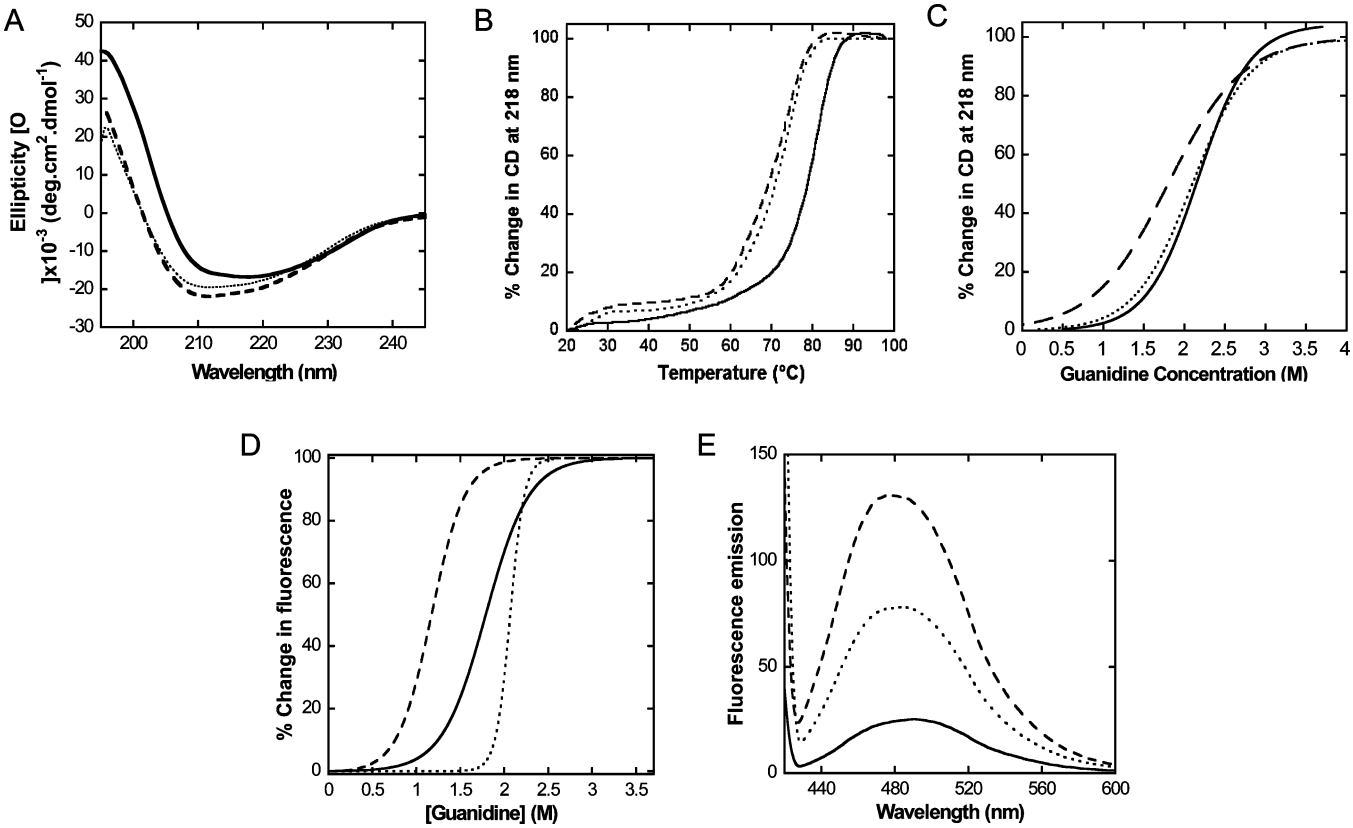


FIGURE 3: Truncations of the C-terminal residues 105−114 alter the tertiary structure of MIF and decrease its stability: solid line, wt huMIF; dashed line, ΔC5 huMIF$_{1-109}$; dotted line, ΔC10 huMIF$_{1-104}$. (A) Far UV/CD spectra of wt huMIF (17 $\mu$M), ΔC5 huMIF$_{1-109}$ (25 $\mu$M) and ΔC10 huMIF$_{1-104}$ (20 $\mu$M) in PBS 1X, pH 7.4. (B) Thermal denaturation of wt huMIF, ΔC5 huMIF$_{1-109}$ and ΔC10 huMIF$_{1-104}$. (C) GdnHCl-induced unfolding of wt huMIF, ΔC5 huMIF$_{1-109}$ and ΔC10 huMIF$_{1-104}$ monitored by far UV/CD (218 nm) (C) and fluorescence (D). All unfolding studies were performed at protein concentration of 14 $\mu$M. The change in fluorescence as a function of GdnHCl was monitored at 342 nm for wt huMIF, 350 nm for ΔC5 huMIF$_{1-109}$ and 312 nm for ΔC10 huMIF$_{1-104}$ using an excitation wavelength of 280 nm. (E) ANS binding to wt huMIF, ΔC5 huMIF$_{1-109}$ and ΔC10 huMIF$_{1-104}$ monitored by ANS fluorescence emission at 490 nm (excitation at 410 nm).

wt, ΔC5 huMIF$_{1-109}$, and ΔC10 huMIF$_{1-104,}$ respectively. Using the partial specific volume calculated from the amino acid composition, we obtained molecular weights of 35.4 kDa, 35.9 kDa and 33.8 kDa for wt, ΔC5 huMIF$_{1-109}$, and ΔC10 huMIF$_{1-104}$ respectively. Thus, our findings are fully consistent with a strongly associated trimeric quaternary structure of wt, as reported previously (*36, 49*), and mutant proteins. The slight decrease in the sedimentation coefficient values for the carboxy deleted proteins may reflect the small change in molecular weight and/or altered conformational properties of the mutants. In the case of the ΔC10 huMIF$_{1-104}$, two additional minor species with average *s* values of 1.5 S (±0.1 S) and 5 S (±0.1 S) corresponding to monomeric and higher order aggregates were consistently detected in all ΔC10 huMIF$_{1-104}$ samples. These results suggest that the ΔC10 huMIF$_{1-104}$ trimer exhibits slight decreased stability and may undergo aggregation upon dissociation into monomers. To determine if the effect of C-terminal truncation on MIF oligomerization is concentration dependent, we performed sedimentation velocity studies on all three proteins over the concentration range of 2.5−50 $\mu$M. At all concentrations, wt and C-terminal mutants sedimented predominantly as a single species with *s* values and molecular masses corresponding to those of the corresponding trimer (Figure S4, see Supporting Information).

To further probe the effect of C-terminal deletions on the oligomerization state of MIF, we determined the quaternary structure distribution of wt, ΔC5 huMIF$_{1-109}$ and ΔC10 huMIF$_{1-104}$ by analytical SEC and native PAGE gel electrophoresis. In nondenaturing gels wt huMIF migrated as two bands, whereas ΔC5 huMIF$_{1-109}$ and ΔC10 huMIF$_{1-104}$ run as a single band. Both mutants exhibited quite similar electrophoretic mobility to one of the bands of wt MIF (Figure 4C). It is noteworthy that removing the C-terminal amino acids 105−114 does not alter the charge distribution and PI of the mutants relative to the wt protein. Analysis of the same samples by analytical SEC (Superdex 75) is consistent with the native PAGE and demonstrates that wt huMIF elutes mainly as two peaks with elution volumes of 13.8 and 15.8 mL (Figure 4D). The C-terminal deletion mutants ΔC5 huMIF$_{1-109}$ and ΔC10 huMIF$_{1-104}$ elute predominantly as a single peak with an elution volume of 11.5 mL. To better assess the true oligomerization state of wt and C-terminal mutants the samples corresponding to each peak were reinjected into a Superdex 75 column and analyzed by light scattering upon elution (Figure 5). These studies show that the eluting species do not interconvert in the time scale of our experiments and confirmed that all of the peaks correspond to trimeric forms of MIF (Figure 5). The fact that the observed differences in catalytic activity, electrophoretic mobility, SEC elution profiles, and thermodynamic stability between the C-terminal deletion mutants occur in the absence of any change in the oligomerization state of the protein suggests that removal of the C-terminal residues

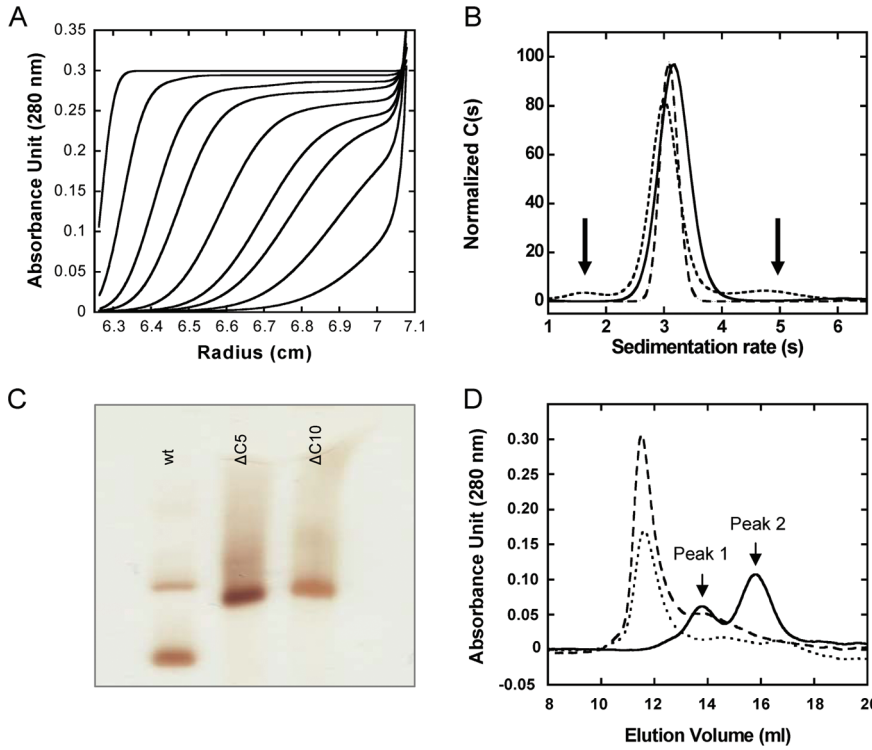


FIGURE 4: C-Terminal truncations do not affect the quaternary structure of huMIF. (A) Sedimentation velocity profiles of wt huMIF (12 $\mu$M). Scans for analysis were recorded every 3 min; for clarity, only 9 representative scans 20−30 min apart are shown. (B) Sedimentation coefficient distributions were obtained from analysis of the sedimentation profiles of wt and C-terminal mutants at 12 $\mu$M using the $C(s)$ distribution as a variant of Lamm equation solutions using SEDFIT as described in Materials and Methods: solid line, wt huMIF; dashed line, $\Delta$C5 huMIF$_{1-109}$; dotted line, $\Delta$C10 huMIF$_{1-109}$:. (C) Native PAGE gel of purified wt huMIF, $\Delta$C5 huMIF$_{1-109}$, and $\Delta$C10 huMIF$_{1-104}$. (D) Analytical SEC profiles of wt huMIF (solid line), $\Delta$C5 huMIF$_{1-109}$ (dashed line) and $\Delta$C10 huMIF$_{1-104}$ (dotted line).

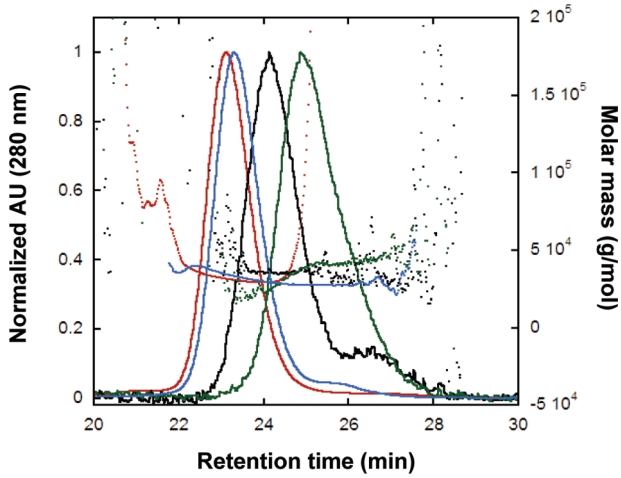


FIGURE 5: Wt and C-truncated huMIF exist as stable trimers. Light scattering analyses of the reinjected peak 1 (black line) and peak 2 (green line) from preparative SEC of wt huMIF, $\Delta$C5 huMIF$_{1-109}$ (blue line) and $\Delta$C10 huMIF$_{1-104}$ (red line). The individual data points show the molecular weight at each point in the chromatogram.

110−114 or 105−114 results in significant changes in the tertiary structure of the trimer.

*Disruption of the C-Terminal $\beta$-Hairpin Produces Similar Effects As Removal of the C-Terminal Residues 105−114.* To determine whether the loss of catalytic activity and decreased thermodynamic stability in the case of both deletion mutants is due to removal of these residues or simply disruption of the C-terminal $\beta$-hairpin, we generated an MIF variant (P107) in which a proline residue was inserted at position 107 (Figure 6). This insertion disrupts key hydrogen bonding interactions involved in the stabilization of the C-terminal $\beta$-hairpin (Figure 6A). Similar to the C-terminal deletion mutants, the P107 variant showed a CD spectrum shifted toward lower wavelengths (Figure 6B), consistent with loss of the C-terminal $\beta$-hairpin, and a decreased thermodynamic stability (Figure 6C) as assessed by the $T_m$ value (72 °C). On the other hand P107 huMIF sedimented predominantly as a single species with sedimentation coefficient of 3.0 ± 0.1 S (MW = 38.12 kDa) by sedimentation velocity (Figure 6D). Finally, biochemical studies revealed that of P107 variant exhibits very minimal catalytical activity (Figure 6E).

*C-Terminal Truncations Result in Significant Perturbations of the Tertiary Structure of MIF without Affecting the Oligomerization State of the Protein.* To test our hypothesis and directly probe the influence of the C-terminal truncation on the structure of MIF, we applied NMR spectroscopy to wt and mutant MIF. The 2D $^{1}H-^{15}N$ HSQC of wt huMIF closely resembles previously observed NMR spectra (*30, 50*) (Figure 7A). 100 out of 107 expected signals arising from backbone amide−amide proton pairs could be assigned on the basis of published resonance assignments (*30, 50*) (Figure 7A). Deletion of 10 residues at the C-terminus induced dramatic changes in the NMR spectra (Figure 7A). The number of backbone signals was reduced to ~70. Almost all resonances were broadened and shifted compared to wt MIF. Using 3D HNCA experiments, 26 of the backbone resonances could be sequence specifically assigned. The residues for which sequence specific assignments could be obtained were distributed along the primary sequence. For

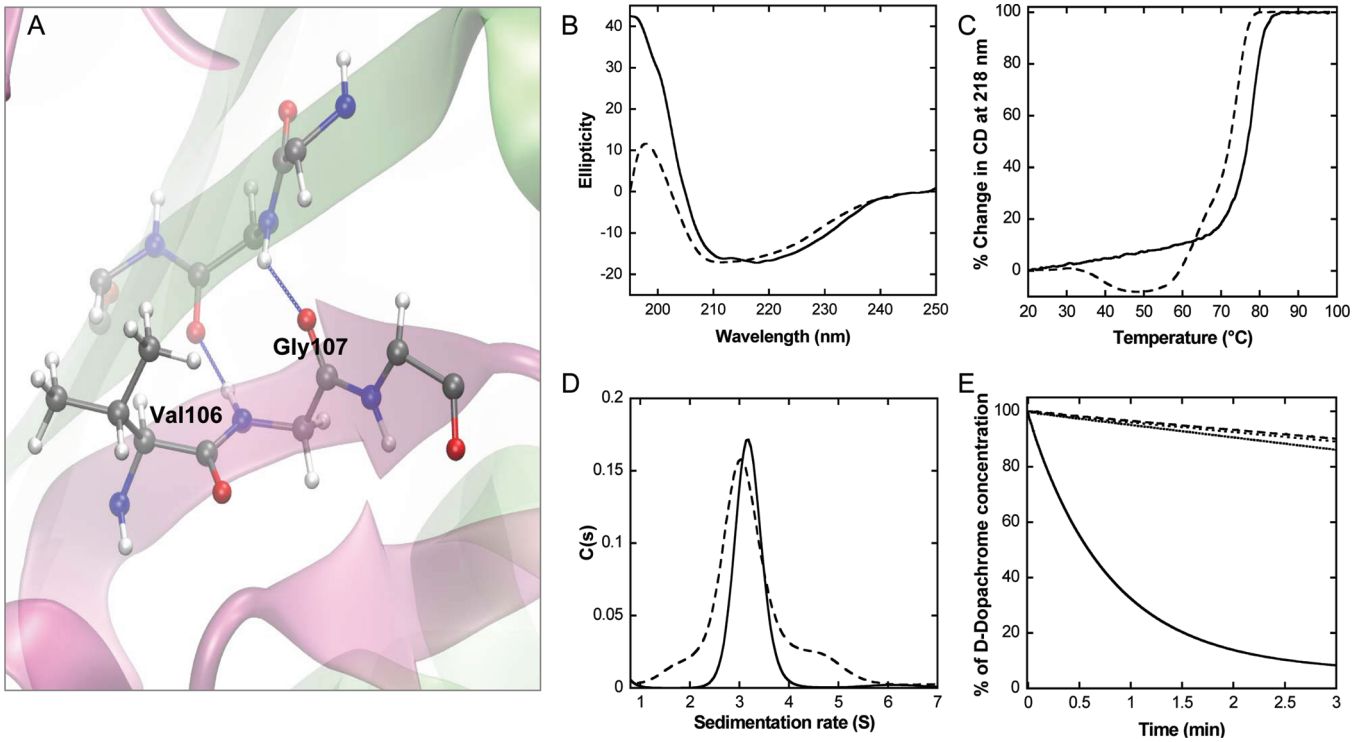


FIGURE 6: Disruption of the C-terminal $\beta$-hairpin produces similar effects as removal of the C-terminal residues 105−114. (A) Pro107 variant was generated by insertion of a proline between residues Val106 and Gly107 to disrupt key hydrogen bonding interactions involved in the stabilization of the C-terminal $\beta$-hairpin. Far UV/CD spectra (B) and thermal denaturation (C) of wt huMIF (solid line) and P107 huMIF (dashed line). (D) Sedimentation coefficients distributions of wt huMIF (solid line) and P107 huMIF (dashed line). Far UV/CD, thermal stability and sedimentation velocity experiments were performed on the same dialyzed sample at 15 $\mu$M in PBS 1X. (E) D-Dopachrome (278 $\mu$M) tautomerization in the presence of 19 nM of wt huMIF (solid line), 25 nM of P107 huMIF and 90 nM P107 huMIF (dotted lines). Dashed line corresponds to the substrate in the absence of MIF.

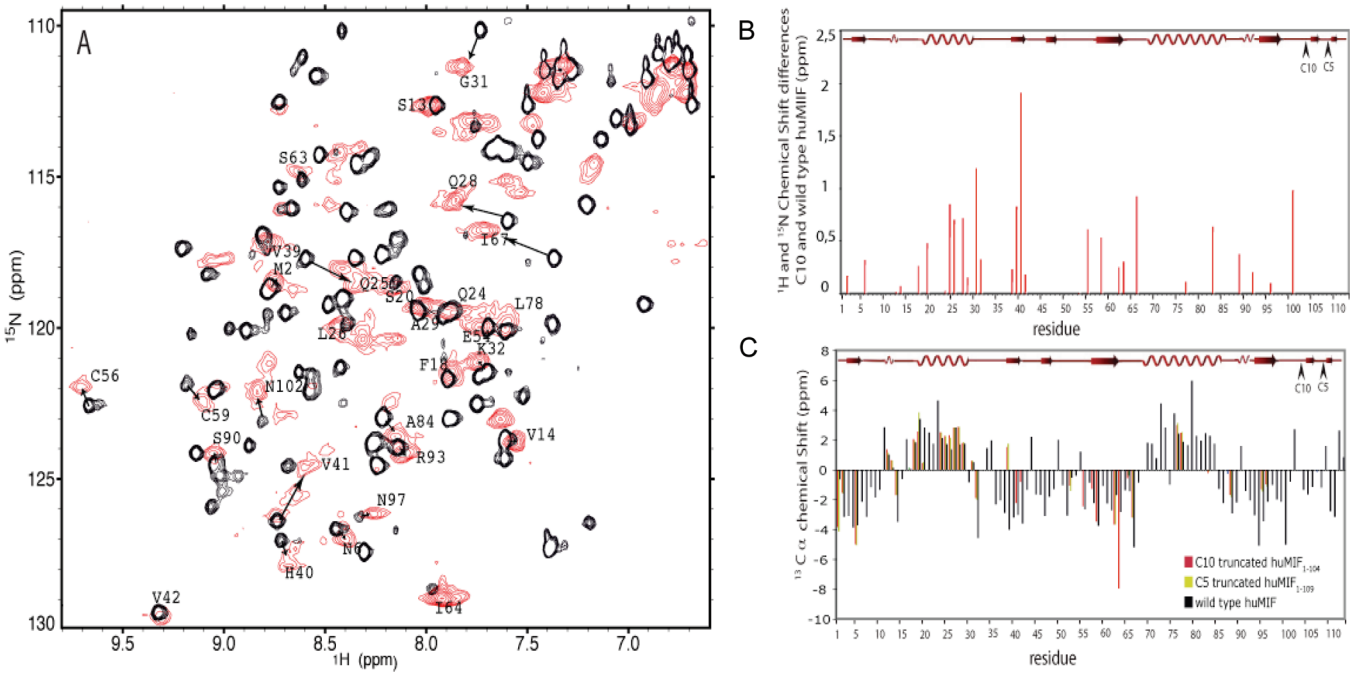


FIGURE 7: Secondary structure of wt, ΔC5 huMIF$_{1-109}$ and ΔC10 huMIF$_{1-104}$. (A) Superposition of two-dimensional $^{1}$H−$^{15}$N HSQCs of wt (black) and ΔC10 huMIF$_{1-104}$ (red). Resonance assignments of strongly shifting resonances are indicated. (B) $^{1}$H/$^{15}$N chemical shift differences between wt and ΔC10 huMIF$_{1-104}$. (C) Cα secondary chemical shifts observed in wt (black), ΔC5 huMIF$_{1-109}$ (green) and ΔC10 huMIF$_{1-104}$ (red). Secondary structure elements observed in the crystal structure of wt MIF are indicated.

Gly51, two signals were observed suggesting that this residue exchanges between two different conformations.

NMR chemical shifts, in particular of Cα atoms, are very sensitive probes of secondary structure. These shifts show distinct deviations from random coil values for both wt and mutants MIF (Figure 7C). In the case of wt huMIF, the Cα secondary structure-dependent chemical shifts are in good agreement with the location of secondary structure elements observed in the crystal structure of wt MIF (*27*). In ΔC5 and ΔC10 truncated huMIF, very similar Cα secondary

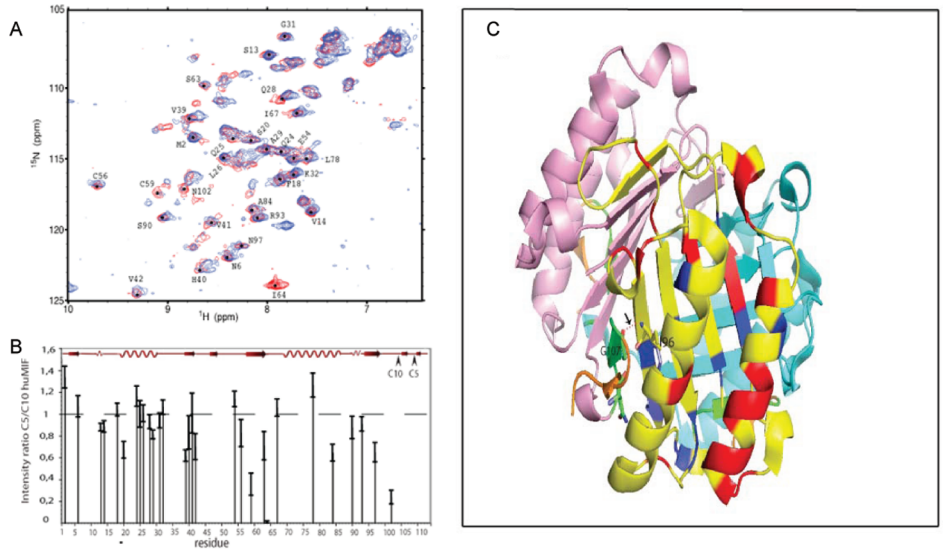


FIGURE 8: Comparison of the structural properties of ΔC5 huMIF$_{1-109}$ and ΔC10 huMIF$_{1-104}$ with single-residue resolution. (A) Superposition of $^{1}$H−$^{15}$N HSQCs of ΔC5 huMIF$_{1-109}$ (blue) and ΔC10 huMIF$_{1-104}$ (red). Resonances that could be assigned are labeled with residue number. (B) Ratio of signal intensities of resonances observed for ΔC5 huMIF$_{1-109}$ and ΔC10 huMIF$_{1-104}$ in $^{1}$H−$^{15}$N HSQC spectra. Secondary structure elements observed in the crystal structure of wt MIF are indicated. (C) Ribbon diagram of the crystal structure of MIF (pdb 1GD0) with residues that could be assigned in ΔC10 huMIF$_{1-104}$ in red. In blue, residues are highlighted for which the intensity ratio shown in (B) was below 0.8. β-Strands β6 and β7 are shown in green and orange. Gly107 and Ile96 that form a hydrogen bond are highlighted.

structure-dependent chemical shifts were observed for those residues that were visible in the NMR spectra and that could be sequence specifically assigned (Figure 7C). In all β-strands except β3 and all α-helices except helix H2 at least a single residue could be assigned in the deletion mutants. This indicates that the secondary structure elements in ΔC5 huMIF$_{1-109}$ and ΔC10 huMIF$_{1-104}$ are overall retained in agreement with CD measurements, as also found in our MD runs (see below). In β-strand β5 the observed secondary chemical shifts are smaller than those observed for the wt protein indicating that the last β-strand before the position of truncation is destabilized. This is also found in our MD run, where residues 95−97 temporarily lose the β-sheet conformation (see below).

The 2D $^{1}$H−$^{15}$N HSQC spectra of both C-truncated huMIF were very similar (Figure 8A). Both the positions and line widths of signals were very similar. Interestingly, the signal of Ile64, which was not visible for ΔC5 huMIF$_{1-109}$, was observable in the HSQC of ΔC10 huMIF$_{1-104}$ at a similar position as observed in wt huMIF. In addition, some other residues showed lower signal intensities in ΔC5 huMIF$_{1-109}$ when compared to ΔC10 huMIF$_{1-104}$ (Figure 8B). In particular, β-strands β4 (residues C59, S63 and I64) and β5 (residue N97) were affected by increased chemical exchange in ΔC5 huMIF$_{1-109}$. Note that reducing the concentration of ΔC10 huMIF$_{1-104}$ from 60 to 10 μM did not strongly change the position and line width of signals in the 2D $^{1}$H−$^{15}$N HSQC, suggesting that the changes observed in the NMR-spectra of MIF upon truncation are not due to an altered aggregation propensity.

*Molecular Dynamics Simulations.* In silico studies were employed to provide insight into the structural consequences of deleting the C-terminal residues 105−114, and 110−114 and their contribution to the structure and stability of huMIF. Three independent MD simulations of 10 ns were performed for the wt huMIF trimer and the C-terminal deletion mutants ΔC5 huMIF$_{1-109}$ and ΔC10 huMIF$_{1-104}$. Although the simulation times are relatively short, we observe, for both forms of C-truncated huMIF, an increase of the values reached by the rmsd (1.8 for the wt huMIF, against 2.7 Å for ΔC5 huMIF$_{1-109}$ and 2.3 Å for ΔC10 huMIF$_{1-104}$) (Figure 9A). In the case of ΔC5 huMIF$_{1-109}$, the profile of the rmsd is slightly divergent, which suggests that the structure might undergo further conformational modifications on a longer time-scale. The root-mean-square fluctuations of the residues in both mutant huMIFs are qualitatively similar to those of the wt, but show higher deviations in the region between residues 65 and 90, corresponding to helix H2 (Figure 1B), suggesting accumulation of mechanical strain in that region. These findings are related to the removal of the native salt bridge occurring between the carboxyl group of the C-terminal residue Ala114 of one monomer and the side-chain of Arg73, located at the second turn of the helix H2 of the neighboring monomer. The carboxy-terminal region also shows a much higher mobility than in the wt huMIF (Figure 9B).

Although deletion of C-terminal β-strands is expected to disrupt all the local intersubunit interactions, including the C-terminal salt bridge, the molecular simulation data revealed that the C-terminal salt bridge is maintained in both truncated huMIF mutants (Figure 10A−C). In ΔC5 huMIF$_{1-109}$ the new C-terminal residue is Asn109; the distance in the wt trimer (*27*) between the C-terminus of Asn109 and the side chain of Arg73 is ∼12 Å. However, upon deletion of the last 5 amino acids, our simulations show that a new salt bridge can still be formed. This is facilitated by rotation of the Arg73 side chain (Figure 10B), which can bring the two charged residues back to the typical salt-bridge distances (Figure 10D). In the case of ΔC10 huMIF$_{1-104}$, the C-terminal residue Ala104, which in wt huMIF is located at the loop that links the C-terminal hairpin to the rest of the protein, is still capable of forming a salt bridge with Arg73 (Figure 10C) (initial crystallographic distance in the wt between Ala104 and Arg73 is 7 Å). Statistical distribution

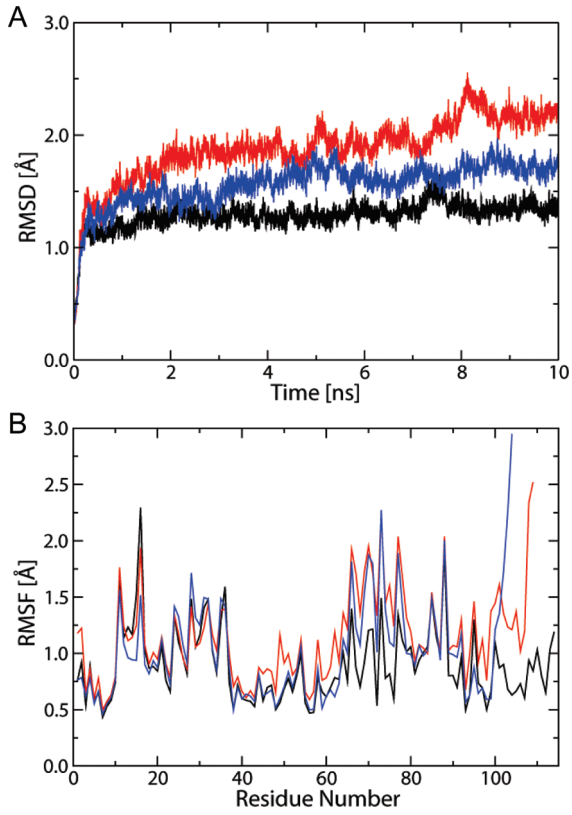


FIGURE 9: Root-mean-square deviations (rmsd) of the backbone atoms (A) and root-mean-square fluctuations (rmsf) per amino acid (B) of wt huMIF and C-terminal truncated mutants. Black line: wt protein. Red line: ΔC5 huMIF$_{1-109}$. Blue line: ΔC10 huMIF$_{1-104}$.

of the C-terminus-Arg73 side-chain distances in all 3 proteins (Figure 10D) shows clearly a clear sharp peak at around 4−4.5 Å. Integration of this first peak confirms that wt huMIF has the most stable ionic interaction at the C-terminus (i.e., the salt bridge forms during more than 70% of the total MD simulation time (10 ns)); ΔC5 huMIF$_{1-109}$ shows a less stable interaction with the salt bridge being formed during the 56% of the total MD simulation time, while ΔC10 huMIF$_{1-104}$ is only marginally more stable than ΔC5 huMIF$_{1-109}$ (59% of the total MD simulation time). Due to the topological proximity of the C-terminus to Arg73 in both C-truncated mutants, the retained salt bridge causes an accumulation of mechanical strain in the helix H2 (Figure S2; see Supporting Information).

*MD Simulations Support a Linkage between the Conformational Flexibility of the C-Terminus and Catalytic Activity of MIF.* The catalytic pocket of huMIF is located at the interface between two monomers. The high resolution X-ray structure of MIF bound to its unnatural substrate hydroxyphenyl pyruvate (HPP) in the catalytic active site reveals that interactions with the substrate involve amino acids from two adjacent monomers, more specifically Pro1, Lys32 and Ile64 from one monomer and Tyr95 and Asn97 from the neighboring monomer. As the protein scaffold is rather rigid, and does not undergo major conformational changes upon substrate binding, the orientation of these residues in the wt apoprotein in the X-ray structure is very similar to that in the protein/HPP complex, and is conserved during the 10 ns of our MD simulations.

The catalytic pocket of huMIF is topologically located next to the salt bridge involving Arg73. Our simulations show that the mutated forms of huMIF undergo strong conformational changes in the catalytic pocket. In particular, in both mutants the helix H2 bends, losing the α helix for a 3-10 helical or a coil structure, between Gln71 and Ser76 (Figure S2; see Supporting Information). The orientations of side chains of residues involved in forming the catalytic active site are dramatically altered in both carboxy truncated mutants and predict drastic effects on the tautomerase activity of these proteins.

Superimposition of the structures of wt and C-terminal deletion mutants shows that both ΔC5 huMIF$_{1-109}$ and ΔC10 huMIF$_{1-104}$ structures deviate from the wt huMIF one (rmsd of 3.60 Å and 2.18 Å respectively) (Figure 11). During our MD simulations, we observe an overall enlargement of the catalytic pocket in ΔC5 huMIF$_{1-109}$ (Figure 11A). This event was monitored by computing the radial distribution function (RDF) between the nitrogen atom of Pro1, located approximately at the center of the catalytic pocket, and the water oxygen atoms. Spatial integration of the RDF makes evident that the average number of water molecules in the pocket of ΔC5 huMIF$_{1-109}$ increases with respect to the wild type (7.5 and 8.7 water molecules for the wt huMIF and ΔC5 huMIF$_{1-109}$, respectively) (Figure 11C,D). In the case of ΔC10 huMIF$_{1-104}$, we instead observe a reduction of the solvent-accessible space in the catalytic pocket (Figure 11B−D) (6.4 water molecules). In addition, we report a different packing of the side-chain of Met101 (Figure 10E−G), which temporarily intercalates between the catalytic residues Tyr95 and Asn97 in the binding site. Such intrusion clearly interferes with the binding properties of the substrate, since the cleft between Tyr95 and Asn97 is typically occupied by its aromatic ring. Furthermore, both superimpositions of the mutant structures to the wild type one, show a flipping of Asn97 side chain in both C-truncated huMIF forms with respect to wt huMIF (Figure 11A,B), which implies a dramatic modification of the characteristic hydrogen-bond patterns in the catalytic pocket. The radical change of the relative positions of the catalytic amino acids must have a strong disruptive impact on the enzymatic activity of the protein, as assessed in our experiments. It is noteworthy that significant structural deviations occur during the simulation in the region comprising residues 50−104 of the C-terminal mutants (Figure 9) suggesting that decreased stability and loss of catalytic activity may be the result of both local and global conformational changes in the trimer.

## DISCUSSION

In this study, we sought to provide some insight into the structural and molecular determinants involved in regulating the structure and activity of MIF. We focused on elucidating the relative contribution of the various intersubunit interactions, suggested by the X-ray and MD-solution structures of the trimer, on the structural and functional properties of MIF.

The C-terminal region of MIF, in particular residues 105−114, is highly conserved (>95%) across different species (Figure 1D), suggesting that it may play critical roles in modulating the structure and activity of MIF *in vivo*. This notion is supported by high-resolution X-ray structures of MIF demonstrating that this region is highly ordered and participates in several intersubunit interactions at the

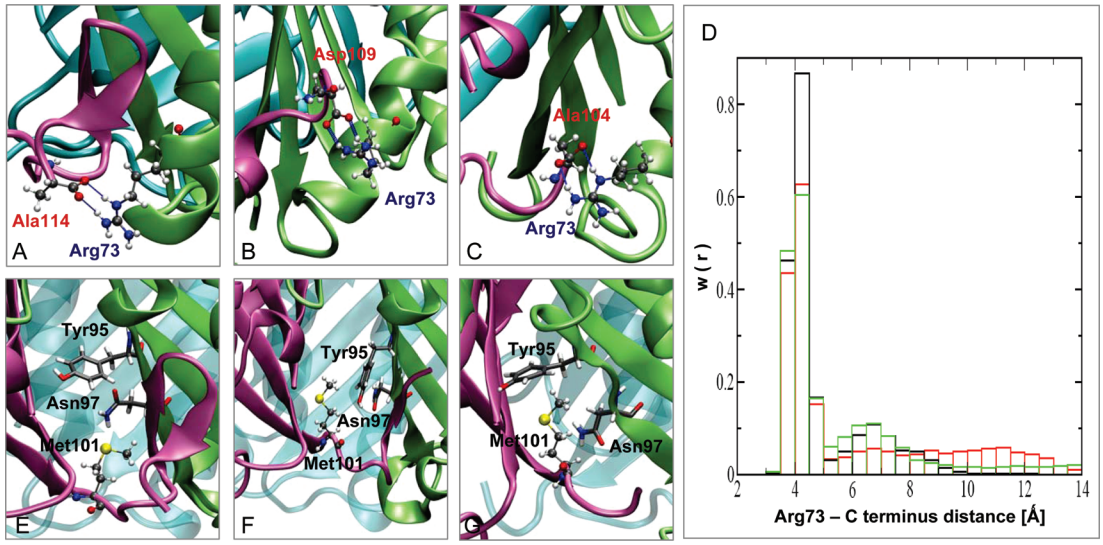


FIGURE 10: The salt bridges between the C-terminal carboxylate group and Arg73 are retained in wt (A) and both C-terminal deletion mutants (B, C). The C-terminal residue and Arg73 are drawn in ball-and-sticks; the rest of the protein is represented by a cartoon. The three monomers are colored in cyan, green and magenta, respectively. Panel (D) represents the statistical distribution of the salt-bridge distance. Distance between Cα atom of arginine and the carbonyl C atom of the C-terminal residue is reported on the *x*-axis. The relative probability density is reported on the *y*-axis. The histograms correspond to the wt huMIF (black), ΔC5 huMIF$_{1-109}$ (red) and ΔC10 huMIF$_{1-104}$ (green). Panels (E−G) represent the Met101 position in wt huMIF, ΔC5 huMIF$_{1-109}$ and ΔC10 huMIF$_{1-104}$ respectively. Met101 is drawn in ball-and-sticks, Tyr95 and Asn97 are drawn in licorice, and the rest of the protein is represented by a cartoon. The three monomers are colored in cyan, green and magenta, respectively.

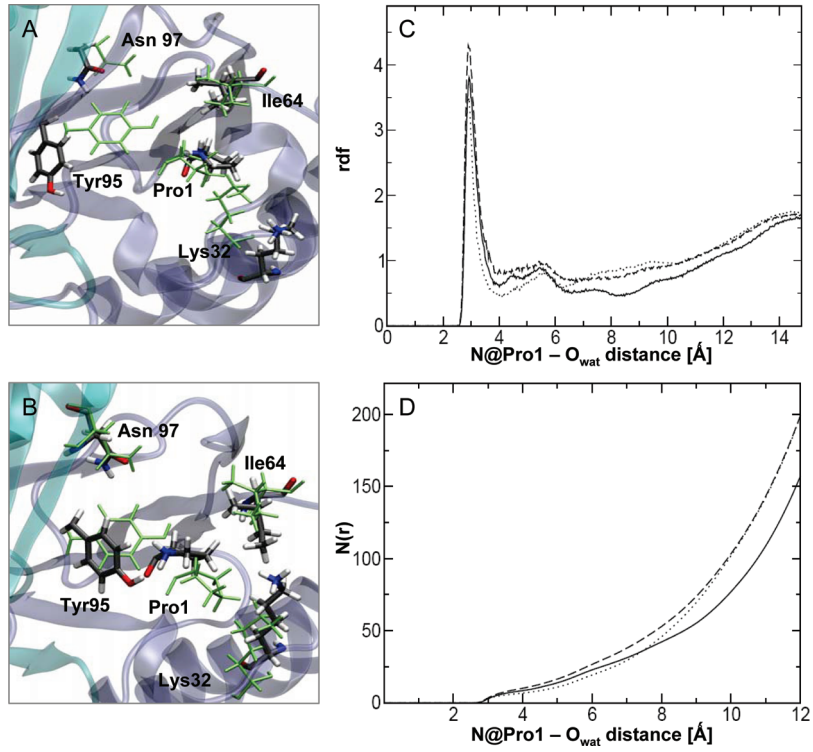


FIGURE 11: Geometrical distortion of the active-site pocket induced by removal of the C-terminal β-strands. Superimposition of the binding site residues in wt huMIF to the same residues in ΔC5 huMIF$_{1-109}$ (panel A) and ΔC10 huMIF$_{1-104}$ (panel B). Wt huMIF catalytic residues are colored in green, and those of the mutated forms are colored according to the standard element code (blue, nitrogen; red, oxygen; gray, carbon; blank, hydrogen). The two adjacent monomers where the binding residues are located are shown with cartoon, and colored in cyan and ice-blue respectively. Only monomers from the wt structure are represented for simplicity. (C, D) Radial distribution functions between Pro1 backbone N atom and water oxygen atoms. The rdf's (C) and their spatial integrals (D) are reported for the wt huMIF (solid line), ΔC5 huMIF$_{1-109}$ (dashed line) and ΔC10 huMIF$_{1-104}$ (dotted line) proteins.

monomer−monomer interface (Figure 1B). Furthermore, previous structure activity studies have suggested that this region may play an important role in modulating the stability and oligomerization of MIF (*29, 31*). We used a battery of biophysical techniques, biochemical assays and molecular dynamics simulations to characterize deletion and insertion mutants of MIF designed to probe the role of the C-terminal region (residues 105−114) in modulating the conformational flexibility, tertiary structure, oligomerization state, catalytic activity, and receptor binding properties of MIF. Our results

provide new insight into the structural consequences of disrupting and/or removing this region and molecular basis underlying its role in modulating the tertiary structure, conformational flexibility and activity of MIF.

The catalytic activity of MIF is oligomerization-dependent; the active sites are formed at the monomer−monomer interfaces. Therefore, conformational changes in regions involved in trimer formation and stability should influence MIF enzymatic activity. In this study, we demonstrate that the C-terminal region of MIF contributes to tertiary structure stabilization and thermodynamic stability of MIF and plays a critical role in modulating its catalytic activity. Removal of the last 5−10 (110−114 or 105−114) C-terminal amino acid residues of MIF has been reported to lead to reduction or loss of MIF catalytic activity (*29, 31*). In our hands, we consistently observed that deletion of the C-terminal region abolishes MIF tautomerase activity. Considering the active site of MIF and its location relative to the C-terminus of each monomer (Figure 1C), there are two possible explanations for the loss of activity upon deleting the last 5−10 C-terminal residues of MIF: (i) dissociation of the trimer or (ii) or changes in tertiary structures and dynamics, in particular involving the active site, induced by disruption of the intersubunit $\beta$-sheet formed by C-terminal strand $\beta$6 of one monomer and $\beta$5 strand of the neighboring monomer. To test these possibilities, we determined the effect of the C-terminal deletions on the oligomeric state (by sedimentation velocity analytical ultracentrifugation, gel filtration, light scattering and native gel electrophoresis), secondary structure (far UV/CD), and tertiary structure (fluorescence spectroscopy and NMR) of wt and both mutants. Sedimentation velocity analytical ultracentrifugation studies demonstrate that both mutants sediment predominantly as a single species with sedimentation coefficient and molecular weight values (Figure 4B) corresponding to that of the trimer, suggesting that C-terminal deletions do not significantly affect the quaternary structure (trimer) of MIF. It is noteworthy that the C-terminal deletion mutants exhibited increased propensity to form irreversible aggregates with time and higher monomer contents relative to wt MIF, indicating that disruption of this region may alter the kinetic stability of the trimer.

*Removal of the C-Terminal Strands β6 and/or β7 Alters the Conformational Properties of the MIF Trimer.* Despite the similarity in sedimentation properties among the wt and C-terminal deletion mutants, the gel filtration profiles and electrophoretic mobility in native gels of both mutants were distinct from those of the wt protein. Wt huMIF elutes as two main overlapping peaks, whereas both mutant elute as a single peak (Figure 4D). In native gels, wt MIF runs as two distinct bands, whereas both C-terminal deletion mutants run as a single band with electrophoretic mobility similar to the fast moving band of wt huMIF. Light scattering measurements proved that both peaks corresponding to wt huMIF as well as C-terminal deleted mutants correspond to the trimeric state of MIF. Together these data suggest that MIF trimer exists as a mixture of at least two different, but closely related, conformational states and that the tertiary structure of the trimer is altered by conformational changes and/or disruption of the C-terminal region 105−114.

To better understand the structural basis underlying the changes in gel filtration and electrophoretic mobility as well as the loss of catalytic activity upon deletion of the C-terminal $\beta$-strands ($\beta$6 and/or $\beta$7), we probed the secondary and tertiary structure of wt and C-terminal deletion mutants by far-UV/CD, NMR spectroscopy and molecular dynamics. Although the CD spectra of the mutants are very similar to that of the wt and consistent with the loss of $\beta$-sheet structure upon deletion of the $\beta$-strands $\beta$6 and/or $\beta$7, the NMR spectra unambiguously show that deletion of the five C-terminal residues strongly destabilizes almost the entire protein, such that the backbone is strongly involved into chemical exchange. These findings are consistent with the decreased thermodynamic stability of both mutants relative to the wt protein (Figure 3). Deletion of the $\beta$6 and $\beta$7 was expected to result in the loss of hydrogen bonding and salt-bridge intersubunit interaction and lead to increased destabilization relative to the ΔC5 mutant, which was designed to disrupt the salt-bridge interaction while maintaining the intersubunit interactions between $\beta$6 from one monomer and $\beta$5 of the neighboring monomer. Although both mutants exhibited decreased thermodynamic stability relative to wt huMIF, truncation of the C-terminal $\beta$-hairpin has less effect on the stability of MIF than the deletion of the $\beta$-strand $\beta$7. ΔC10 $huMIF_{1-104}$ was more stable than ΔC5 $huMIF_{1-109}$ to thermal and GdnHCl induced denaturation and exhibited reduced binding to ANS, suggesting that changes in tertiary structure induced by removal of the C-terminal $\beta$-hairpin ($\beta$6 and $\beta$7) induces more stable interactions within the protein that compensate for some of the trimer stabilizing interactions involving the $\beta$-strands $\beta$6 and $\beta$7 lost. Furthermore, our molecular dynamics simulations demonstrate that the salt bridge at the carboxy-terminus still forms in both mutants and may constitute a major structural element in modulating the oligomerization and stability of MIF. However, distance distribution of the salt bridge at the carboxy terminus is marginally higher in ΔC10 $huMIF_{1-104}$ compared to ΔC5 $huMIF_{1-109}$ (Figure 10) consistent with the experimental data demonstrating that ΔC5 $huMIF_{1-109}$ is less stable than ΔC10 $huMIF_{1-104}$.

NMR chemical shifts are highly sensitive to the chemical environment and provide excellent probes for the secondary and tertiary structure of proteins. The large spread of signals observed in the proton dimension of the NMR spectra of ΔC5- and ΔC10-truncated MIF demonstrated that the deletion mutants retain a globular three-dimensional fold (Figures 7A, 8A). Proton amide chemical shifts downfield of 8.5 ppm report on the presence of $\beta$-strands in ΔC5- and ΔC10-truncated MIF in agreement with CD spectroscopy. On the other hand, the dramatic changes in the NMR spectra indicate that deletion of five or ten residues at the C-terminus not only affects the local environment, but influences all the structure of MIF. The line width of NMR signals depends on the molecular weight of the protein as well as the internal flexibility of residues. Increasing molecular weight causes line broadening whereas higher internal mobility leads to narrower NMR signals. On the other hand, chemical exchange between different conformations that is intermediate on the NMR time scale leads to broadening of NMR signals. Analytical ultracentrifugation showed that ΔC5-truncated MIF retains the trimeric arrangement seen for the wt protein in various crystal structures. Thus, the increased line widths observed for the truncation mutants of MIF are most likely not due to a higher-order oligomeric state of the

protein. At the same time, unspecific aggregation appears not to play a major role as 6-fold reduction of the concentration did not alter the position and line width of signals significantly. The increased line width, as well as the disappearance of 30% of signals and the presence of two conformations for Gly51, rather suggests that truncation of the C-terminus leads to strong chemical exchange within the MIF molecule. The conformational exchange might take place within the subunits but also in the intermolecular interfaces of the MIF homotrimer. Importantly, it was previously shown that protein motions necessary for catalysis are an intrinsic property of the enzyme and may even limit the overall turnover rate (*51*). Therefore the impairment of catalytic activity of MIF might also be a direct consequence of the observed changes in the intrinsic dynamics of truncated MIF.

*Conformational Flexibility of the C-Terminal Region May Be Responsible for the Catalytic and Biological Activities of MIF*. Our results suggest that differences in tertiary structure and intrinsic protein dynamics, rather than oligomeric state, may underlie the loss of activity upon deletion of the C-terminal residues 105−114. Previously it was shown that Pro1 interacts with *p*-hydroxyphenylpyruvate. NMR spectroscopy, however, showed that binding of *p*-hydroxyphenylpyruvate to MIF affects not only the N-terminus of MIF but a much larger set of residues including several residues at the C-terminus (Asn102, Gly107, Trp108, Phe113 and Ala 114) (Figure 1C). These residues cluster around Pro1 but arise partially from different subunits. Interestingly, Ala38 and Ile64 disappeared upon addition of *p*-hydroxyphenylpyruvate and they are also no longer visible upon truncation of MIF at Asn109 (*52*).

To better understand whether the loss of catalytic activity and decreased thermodynamic stability upon deletion of the C-terminal residues 105−114 is due to the truncation or simply disruption of the C-terminal $\beta$-hairpin, P107 was generated. Far UV/CD, AUC and biochemical studies reveal that insertion of proline at this site disrupts the C-terminal $\beta$ hairpin and results in a loss of catalytic activity (Figure 6). Similar to the C-terminal deletion mutants, the P107 variant was enzymatically inactive, exhibited decreased thermodynamic stability and sedimented predominantly as a single species corresponding to the trimer. These findings are consistent with our hypothesis that the conformational flexibility of the C-terminal region, which could also be induced through changes in solution conditions or interactions between MIF and its partners, may act as a molecular switch that regulates the equilibrium between the different trimeric states of MIF, most likely by altering the tertiary structure and/or stability of the trimer.

Although we did not investigate the effect of the C-terminal deletions in regulating the biological activities of MIF, previous studies have shown that similar truncation abolishes the MIF's macrophage activating properties (*29, 31*). If, indeed, truncation of the C-terminus or disruption of its structure leads to reduction or blocking of MIF biological activity, this would suggest that such disrupted activity is linked to the catalytic activity of MIF, which can be verified by mutating the N-terminal proline. An alternative explanation would be that the disrupted biological activity is linked to a specific conformation of the MIF trimer which is accessible to the wt protein but not to the mutants. The fact that at least one of the trimers formed by the wt, albeit a minor species, exhibits similar properties as the C-terminal deletion mutants suggests that this activity may be regulated by factors that influence the conformational flexibility and stability of the trimer. Although our results suggest that the C-terminus of MIF is not involved in receptor (CD74) binding, further studies are required to determine whether these mutations affect huMIF signal transduction necessary for intracellular MIF activity. Given its conformational flexibility and accessibility, it is tempting to speculate that the C-terminus of MIF may play a critical role in modulating specific protein−protein and protein−small molecule interactions or in regulating MIF's interaction with fatty acids and biological membranes.

## CONCLUSION

In this study, we investigated the role of the C-terminal region in modulating the tertiary structure, thermodynamic stability, receptor binding and enzymatic activity of MIF. Two C-terminal deletion and Pro insertion mutants were generated to probe the effect of the various intersubunit interactions involving the C-terminal region comprising the amino acid residues 105−114. Our results suggest that the carboxy-terminal region is required for stabilizing the tertiary structure of MIF and maintaining it in an enzymatically active conformation, but does not play a significant role in modulating the oligomerization (trimer formation) of MIF. Although removal of the C-terminal residues 110−114 or 105−114 has no effect on trimer formation and MIF binding to CD74, it causes significant structural changes in the structure and intrinsic dynamics in most of the protein including active site. These changes resulted in loss of tautomerase activity and suggest a possible role for this region in regulating the conformational flexibility of MIF and fine-tuning its catalytic activity. However, further structure activity studies are required to determine the role of the C-terminal region of MIF in modulating its various biological activities in vivo.

## ACKNOWLEDGMENT

We thank Pinar Karpinar for help with NMR measurements. We would like to thank Dr. Christoph Johann and Dr. Dierk Roessner from Wyatt Technology Europe for performing the light scattering data. We also thank Mr. Bruno Fauvet and the members of the LMNN for the thoughtful discussions.

## SUPPORTING INFORMATION AVAILABLE

One figure illustrating the intersubunit interactions and the rationale for the C-terminal deletion and insertion mutants. One figure illustrating the structural distortion of MIF upon deletion of the C-terminus as visualized by MD simulations. A third figure showing the characteristic contacts of HPP in MIF catalytic pocket. Two additional figures provide analyses of the thermodynamic stability and oligomerization state of MIF using far UV circular dichroism and analytical ultracentrifugation sedimentation velocity at multiple protein concentrations. This material is available free of charge via the Internet at http://pubs.acs.org.

## REFERENCES


1. Calandra, T. (2003) Macrophage migration inhibitory factor and host innate immune responses to microbes. *Scand. J. Infect. Dis. 35*, 573–576.
2. Calandra, T., Echtenacher, B., Roy, D. L., Pugin, J., Metz, C. N., Hultner, L., Heumann, D., Mannel, D., Bucala, R., and Glauser, M. P. (2000) Protection from septic shock by neutralization of macrophage migration inhibitory factor. *Nat. Med. 6*, 164–170.
3. Radstake, T. R., and Bucala, R. (2007) Macrophage migration inhibitory factor and its genetic association with arthritis: a work in progress. *Curr. Rheumatol. Rep. 9*, 343–344.
4. Santos, L. L., and Morand, E. F. (2006) The role of macrophage migration inhibitory factor in the inflammatory immune response and rheumatoid arthritis. *Wien. Med. Wochenschr. 156*, 11–18.
5. Xu, X., Wang, B., Ye, C., Yao, C., Lin, Y., Huang, X., Zhang, Y., and Wang, S. (2008) Overexpression of macrophage migration inhibitory factor induces angiogenesis in human breast cancer. *Cancer Lett. 261*, 147–157.
6. Bucala, R., and Donnelly, S. C. (2007) Macrophage migration inhibitory factor: a probable link between inflammation and cancer. *Immunity 26*, 281–285.
7. Yabunaka, N., Nishihira, J., Mizue, Y., Tsuji, M., Kumagai, M., Ohtsuka, Y., Imamura, M., and Asaka, M. (2000) Elevated serum content of macrophage migration inhibitory factor in patients with type 2 diabetes. *Diabetes Care 23*, 256–258.
8. Hoi, A. Y., Iskander, M. N., and Morand, E. F. (2007) Macrophage migration inhibitory factor: a therapeutic target across inflammatory diseases. *Inflammation Allergy Drug Targets 6*, 183–190.
9. Bacher, M., Meinhardt, A., Lan, H. Y., Dhabhar, F. S., Mu, W., Metz, C. N., Chesney, J. A., Gemsa, D., Donnelly, T., Atkins, R. C., and Bucala, R. (1998) MIF expression in the rat brain: implications for neuronal function. *Mol. Med. 4*, 217–230.
10. Nishibori, M., Nakaya, N., Tahara, A., Kawabata, M., Mori, S., and Saeki, K. (1996) Presence of macrophage migration inhibitory factor (MIF) in ependyma, astrocytes and neurons in the bovine brain. *Neurosci. Lett. 213*, 193–196.
11. Bernhagen, J., Calandra, T., Mitchell, R. A., Martin, S. B., Tracey, K. J., Voelter, W., Manogue, K. R., Cerami, A., and Bucala, R. (1993) MIF is a pituitary-derived cytokine that potentiates lethal endotoxaemia. *Nature 365*, 756–759.
12. Fingerle-Rowson, G., Koch, P., Bikoff, R., Lin, X., Metz, C. N., Dhabhar, F. S., Meinhardt, A., and Bucala, R. (2003) Regulation of macrophage migration inhibitory factor expression by glucocorticoids in vivo. *Am. J. Pathol. 162*, 47–56.
13. David, J. R. (1966) Delayed hypersensitivity in vitro: its mediation by cell-free substances formed by lymphoid cell-antigen interaction. *Proc. Natl. Acad. Sci. U.S.A. 56*, 72–77.
14. Bloom, B. R., and Bennett, B. (1966) Mechanism of a reaction in vitro associated with delayed-type hypersensitivity. *Science 153*, 80–82.
15. Cherepkova, O. A., Lyutova, E. M., Eronina, T. B., and Gurvits, B. Y. (2006) Chaperone-like activity of macrophage migration inhibitory factor. *Int. J. Biochem. Cell Biol. 38*, 43–55.
16. Calandra, T., Froidevaux, C., Martin, C., and Roger, T. (2003) Macrophage migration inhibitory factor and host innate immune defenses against bacterial sepsis. *J. Infect. Dis. 187* (2), S385–390.
17. Pyle, M. E., Korbonits, M., Gueorguiev, M., Jordan, S., Kola, B., Morris, D. G., Meinhardt, A., Powell, M. P., Claret, F. X., Zhang, Q., Metz, C., Bucala, R., and Grossman, A. B. (2003) Macrophage migration inhibitory factor expression is increased in pituitary adenoma cell nuclei. *J. Endocrinol. 176*, 103–110.
18. Takahashi, A., Iwabuchi, K., Suzuki, M., Ogasawara, K., Nishihira, J., and Onoe, K. (1999) Antisense macrophage migration inhibitory factor (MIF) prevents anti-IgM mediated growth arrest and apoptosis of a murine B cell line by regulating cell cycle progression. *Microbiol. Immunol. 43*, 61–67.
19. Kleemann, R., Hausser, A., Geiger, G., Mischke, R., Burger-Kentischer, A., Flieger, O., Johannes, F. J., Roger, T., Calandra, T., Kapurniotu, A., Grell, M., Finkelmeier, D., Brunner, H., and Bernhagen, J. (2000) Intracellular action of the cytokine MIF to modulate AP-1 activity and the cell cycle through Jab1. *Nature 408*, 211–216.
20. Calandra, T., Bernhagen, J., Metz, C. N., Spiegel, L. A., Bacher, M., Donnelly, T., Cerami, A., and Bucala, R. (1995) MIF as a glucocorticoid-induced modulator of cytokine production. *Nature 377*, 68–71.
21. Fingerle-Rowson, G., Petrenko, O., Metz, C. N., Forsthuber, T. G., Mitchell, R., Huss, R., Moll, U., Muller, W., and Bucala, R. (2003) The p53-dependent effects of macrophage migration inhibitory factor revealed by gene targeting. *Proc. Natl. Acad. Sci. U.S.A. 100*, 9354–9359.
22. Rosengren, E., Bucala, R., Aman, P., Jacobsson, L., Odh, G., Metz, C. N., and Rorsman, H. (1996) The immunoregulatory mediator macrophage migration inhibitory factor (MIF) catalyzes a tautomerization reaction. *Mol. Med. 2*, 143–149.
23. Rosengren, E., Aman, P., Thelin, S., Hansson, C., Ahlfors, S., Bjork, P., Jacobsson, L., and Rorsman, H. (1997) The macrophage migration inhibitory factor MIF is a phenylpyruvate tautomerase. *FEBS Lett. 417*, 85–88.
24. Lubetsky, J. B., Swope, M., Dealwis, C., Blake, P., and Lolis, E. (1999) Pro-1 of macrophage migration inhibitory factor functions as a catalytic base in the phenylpyruvate tautomerase activity. *Biochemistry 38*, 7346–7354.
25. Kleemann, R., Mischke, R., Kapurniotu, A., Brunner, H., and Bernhagen, J. (1998) Specific reduction of insulin disulfides by macrophage migration inhibitory factor (MIF) with glutathione and dihydrolipoamide: potential role in cellular redox processes. *FEBS Lett. 430*, 191–196.
26. Kleemann, R., Kapurniotu, A., Frank, R. W., Gessner, A., Mischke, R., Flieger, O., Juttner, S., Brunner, H., and Bernhagen, J. (1998) Disulfide analysis reveals a role for macrophage migration inhibitory factor (MIF) as thiol-protein oxidoreductase. *J. Mol. Biol. 280*, 85–102.
27. Orita, M., Yamamoto, S., Katayama, N., Aoki, M., Takayama, K., Yamagiwa, Y., Seki, N., Suzuki, H., Kurihara, H., Sakashita, H., Takeuchi, M., Fujita, S., Yamada, T., and Tanaka, A. (2001) Coumarin and chromen-4-one analogues as tautomerase inhibitors of macrophage migration inhibitory factor: discovery and X-ray crystallography. *J. Med. Chem. 44*, 540–547.
28. Onodera, S., Suzuki, K., Matsuno, T., Kaneda, K., Kuriyama, T., and Nishihira, J. (1996) Identification of macrophage migration inhibitory factor in murine neonatal calvariae and osteoblasts. *Immunology 89*, 430–435.
29. Bendrat, K., Al-Abed, Y., Callaway, D. J., Peng, T., Calandra, T., Metz, C. N., and Bucala, R. (1997) Biochemical and mutational investigations of the enzymatic activity of macrophage migration inhibitory factor. *Biochemistry 36*, 15356–15362.
30. Muhlhahn, P., Bernhagen, J., Czisch, M., Georgescu, J., Renner, C., Ross, A., Bucala, R., and Holak, T. A. (1996) NMR characterization of structure, backbone dynamics, and glutathione binding of the human macrophage migration inhibitory factor (MIF). *Protein Sci. 5*, 2095–2103.
31. Mischke, R., Gessner, A., Kapurniotu, A., Juttner, S., Kleemann, R., Brunner, H., and Bernhagen, J. (1997) Structure activity studies of the cytokine macrophage migration inhibitory factor (MIF) reveal a critical role for its carboxy terminus. *FEBS Lett. 414*, 226–232.
32. Kleemann, R., Kapurniotu, A., Mischke, R., Held, J., and Bernhagen, J. (1999) Characterization of catalytic centre mutants of macrophage migration inhibitory factor (MIF) and comparison to Cys81Ser MIF. *Eur. J. Biochem. 261*, 753–766.
33. Bernhagen, J., Mitchell, R. A., Calandra, T., Voelter, W., Cerami, A., and Bucala, R. (1994) Purification, bioactivity, and secondary structure analysis of mouse and human macrophage migration inhibitory factor (MIF). *Biochemistry 33*, 14144–14155.
34. Hoffman, D. W., and LD, S. (1991) Isotopic labeling of specific amino acid types as an aid to NMR spectrum assignment of the methione repressor protein. *Tech. Protein Chem. 2* 409–419.
35. Molnar, V., and Garai, J. (2005) Plant-derived anti-inflammatory compounds affect MIF tautomerase activity. *Int. Immunopharmacol. 5*, 849–856.
36. Philo, J. S., Yang, T. H., and LaBarre, M. (2004) Re-examining the oligomerization state of macrophage migration inhibitory factor (MIF) in solution. *Biophys. Chem. 108*, 77–87.
37. Schuck, P. (2000) Size-distribution analysis of macromolecules by sedimentation velocity ultracentrifugation and lamm equation modeling. *Biophys. J. 78*, 1606–1619.
38. Leng, L., Metz, C. N., Fang, Y., Xu, J., Donnelly, S., Baugh, J., Delohery, T., Chen, Y., Mitchell, R. A., and Bucala, R. (2003) MIF signal transduction initiated by binding to CD74. *J. Exp. Med. 197*, 1467–1476.
39. Li, H., Robertson, A. D., and Jensen, J. H. (2005) Very fast empirical prediction and rationalization of protein pKa values. *Proteins 61*, 704–721.
40. Case DA, P. D., Caldwell, J. W., Cheatham, T. E., III, Ross, W. S., Simmerling, C. L., Darden, T. A., Merz, K. M., Stanton, R. V.,

Cheng, A. L., Vincent, J. J., Crowley, M. F., Ferguson, D. M., Radmer, R. J., Singh, U. C., Weiner, P. K., and Kollman, P. A. (1999) *AMBER* 6.

41. Cornell WD, C. P., Bayly, C. I., Gould, I. R., Merz, K. M., Jr., Ferguson, D. M., Spellmeyer, D. C., Fox, T., Caldwell, J. W., and Kollman, P. A. (1995) A second-generation force field for the simulation of proteins and nucleic acids. *J. Am. Chem. Soc. 117*, 5179–5197.
42. Jorgensen WL, C. J., Madura, J. D., Impey, R. W., and Klein, M. L. (1983) Comparison of simple potential functions for simulating liquid water. *J. Chem. Phys. 79*, 926–935.
43. Essman, U, P. L., Berkowitz, M. L., Darden, T., Lee, H., and Pedersen, L. G. (1995) A smooth particle mesh Ewald Method. *J. Chem. Phys. 103*, 8577–8593.
44. Ryckaert JP, G. C., and H J.C., Berendsen. (1977) Numerical integration of the cartesian equations of motion of a system with constraints: molecular dynamics of n-alkanes. *J. Comput. Phys. 23*, 327–341.
45. Suzuki, M., Sugimoto, H., Nakagawa, A., Tanaka, I., Nishihira, J., and Sakai, M. (1996) Crystal structure of the macrophage migration inhibitory factor from rat liver. *Nat. Struct. Biol. 3*, 259–266.
46. Starlets, D., Gore, Y., Binsky, I., Haran, M., Harpaz, N., Shvidel, L., Becker-Herman, S., Berrebi, A., and Shachar, I. (2006) Cell-surface CD74 initiates a signaling cascade leading to cell proliferation and survival. *Blood 107*, 4807–4816.
47. Meyer-Siegler, K. L., and Vera, P. L. (2005) Substance P induced changes in CD74 and CD44 in the rat bladder. *J. Urol. 173*, 615–620.
48. Meyer-Siegler, K. L., Vera, P. L., Iczkowski, K. A., Bifulco, C., Lee, A., Gregersen, P. K., Leng, L., and Bucala, R. (2007) Macrophage migration inhibitory factor (MIF) gene polymorphisms are associated with increased prostate cancer incidence. *Genes Immun. 8*, 646–652.
49. Lashuel, H. A., Aljabari, B., Sigurdsson, E. M., Metz, C. N., Leng, L., Callaway, D. J., and Bucala, R. (2005) Amyloid fibril formation by macrophage migration inhibitory factor. *Biochem. Biophys. Res. Commun. 338*, 973–980.
50. Swope, M. D., Sun, H. W., Klockow, B., Blake, P., and Lolis, E. (1998) Macrophage migration inhibitory factor interactions with glutathione and S-hexylglutathione. *J. Biol. Chem. 273*, 14877–14884.
51. Eisenmesser, E. Z., Millet, O., Labeikovsky, W., Korzhnev, D. M., Wolf-Watz, M., Bosco, D. A., Skalicky, J. J., Kay, L. E., and Kern, D. (2005) Intrinsic dynamics of an enzyme underlies catalysis. *Nature 438*, 117–121.
52. Swope, M., Sun, H. W., Blake, P. R., and Lolis, E. (1998) Direct link between cytokine activity and a catalytic site for macrophage migration inhibitory factor. *EMBO J. 17*, 3534–3541.
53. Humphrey, W., Dalke, A., and Schulten, K. (1996) VMD: visual molecular dynamics. *J. Mol. Graphics 14*, 33–38.
54. Soares, T. A., Lins, R. D., Straatsma, T. P., and Briggs, J. M. (2002) Internal Dynamics and Ionization States of the Macrophage Inhibitory Factor: Comparision Between Wild-Type and Mutant Forms. *Biopolymers 65*, 313–323.

BI800603X